

Developing 3D brain models for cell surface sugar targeting with bio-conjugated nanodiamonds

Mina Ghanimi Fard

Supervisors: Dr Lindsay M. Parker and Prof Nicolle H. Packer

A thesis submitted in partial fulfilment of the requirements for the degree

Master of Research (MRes)



MACQUARIE
University

Department of Molecular Sciences (MolSci)
Macquarie University
25th of October 2018

Acknowledgements

Now that I have reached to this end point of my Master of research inspirational journey, I would like to thank all people who supported me throughout the way. I am grateful for the constant guidance and support of my supervisors, **Dr Lindsay Parker** and **Prof Nicolle Packer**. Molecular science was a journey to the detailed and organized microscopic world of biochemistry and they trained me to explore it, they also showed me the big picture and educated me to think out of the box. Their professional and motivational encouragement was beyond expectation. **Dr Parker** was on her journey of motherhood, but she kept on supporting me by coming to work until her last day of anticipation, and even working from home and visiting me at the university during her maternity leave period. **Prof Packer** also enlightened me with her wealth of knowledge and experience and fuelled my soul with positive energy and enthusiasm. Without the help of these two supervisors I would not be able to gain any of the skills and experiences that I am now proud of.

Dr Liisa Kautto, our lab manager had a great impact on my training and providing me with resources required in the lab. Her kindness and smile were as sweet as the cakes she baked for our gatherings at the university, and as warm as the coffee she made for us when she hosted us in her office.

I would like to also thank the MRes committee team including **Dr Louise Brown**, **A/Prof Bridget Mabbutt**, **Prof Alison Rodger**, **Dr Alf Garcia-Bennett** and **Dr Yuling Wang** for their constant support during this period of MRes project.

I appreciate that **Centre for Nanoscale BioPhotonics (CNBP)** funded me by providing a study space for me, maintaining the labs in which I worked, and paying for my laboratory consumables. CNBP organisers also provided me with a platform to connect with researchers in my field of study Australia wide, and updated my knowledge by weekly seminars. I am thankful for being privileged as a member of the team. I am very thankful for **Dr Mark Hutchinson**, **Prof Ewa Goldys**, **Dr Melodee Trebilcock**, **Dr Kathy, Nicholson**, **Prof Jim Piper**, **Ms Jenny Morcom** and **Mr Tony Crawshaw** for providing this opportunity.

I owe so much to **Dr Nicole Cordina** who gave me hands on experience with bio-conjugation of nanodiamonds and was always there for me, regardless of the time of the day.

Dr Anna Guller and **Dr Annemarie Nadort** supported my 3D work like guiding their own students as two kind collaborators.

I would not be able to have any TEM or confocal microscopy images without the help of **Dr Sue Lindsay, Dr Arthur Chien** and **Dr Chao Shen**. Their welcoming smile at the microscopy unit at Macquarie university turned that cold basement into a warm and pleasing space to work for several hours. **Dr shen** took my TEM images and **Dr Chien** patiently taught me to work with the confocal microscope, Imaris software, FIJI (is just imageJ) program and GraphPad Prism. They were both always there to answer my questions and resolve my problems.

The **Olympus company team** were also kind to me and I appreciate that. They kindly lent their new 60x long working distance objective with silicon oil to me, which helped me take all of my 3D cell culture images. Especially, **Ms Tong Wu** who spent half a day with me to demonstrate how to image with the new FV3000 microscope using my 3D samples and arranging the lens to be delivered to me. Also, **Dr Sheng Le**, for delivering the objective to me and collecting it back personally.

Beside the research project and people who contributed to educate me, I was constantly supported by the campus wellbeing and my beloved counsellor **Dr Michael Fitzpatrick**, who sincerely listened to me when I was feeling down and stressed, empathised with me and gave me heart-warming advices and showed me the way to live with a healthy mentality.

Speaking of feelings and emotions reminds me of the good friendships at Macquarie university that helped me survive in hard times and enjoy my happy times. I was blessed with a number of kind and helpful friends who helped me achieve my goals: **Ms Mahsa Vaez Zadeh**, my closest friend and office mate who also helped me in preparation of the scaffolds and confocal microscopy, and her husband **Mr Ehsan Kachooei**, and all of my dear friends **Ms Sarah Hamzelou, Ms Sally Noushini, Ms Zahra Khabir, Ms Mahdyieh Dashtbani Moghari, Mr. Nima Sayyadi, Ms Minakshi Das, Ms Irene Moroni, Ms Sameera Iqbal, Mr Abdulrahman Shathili, Dr Edward Moh, Ms Sayantani Chatterjee** and her partner **Mr Russel Vincent, Mr Benjamin Ford**, and my close friends for ever **Ms Kamala Pangsatabam** and **Ms Ruchi Dhaval Mehta**.

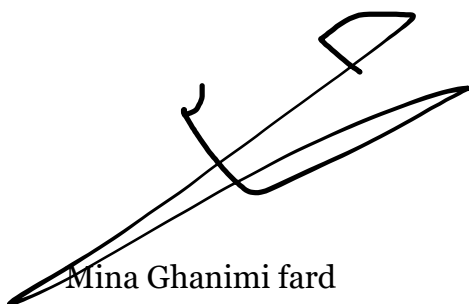
I would like to appreciate my dear family members for always being there for me. My parents **Mr Afshinali Ghanimi fard** and **Ms Farideh Piri**, who have always encouraged me to study and never give up. The only people in the world that would do anything for my success. My younger brother **Mr Amin Ghanimi fard**, who inspired me to work hard and achieve what I want. Last but not least, my dear husband **Mr Ali Omidbakhsh**, who understood me from my deepest within, and shared his endless love with me to the moon and back. I would not be able to accomplish this journey without his patience and understanding.

Declaration

This thesis titled “**Developing 3D brain models for cell surface sugar receptor targeting with bio-conjugated nanodiamonds**” is representative of the research study conducted between January 2018 and October 2018 for the completion of Master of Research degree in Molecular Sciences at Macquarie University, New South Wales, Australia. Where appropriate, work done in collaboration with other groups or individuals and the material provided by them has been acknowledged, and otherwise to the best of my knowledge is my own work and original.

This thesis is formatted according to Master of Research guidelines prescribed by the Faculty of Science & Engineering and Molecular Sciences and no part of this thesis has been submitted for qualification or assessment to any other institution.

Neither ethics approval nor any exempt dealings approval was required for this project.

A handwritten signature in black ink, consisting of several overlapping loops and a long horizontal stroke at the bottom.

Mina Ghanimi fard

Student ID: 42941296

Publications and communications arising from this thesis

I. Publication

Understanding cellular glycan surface in the central nervous system

Mina Ghanimi Fard, Sameera Iqbal, Dr Arun Everest-Dass, Prof Nicolle Packer, Dr Lindsay Parker

This review article was approved on the 10th of September 2018 and resubmitted after revisions to Biochemical Society Transactions journal on the 21st of October 2018. I shared equal authorship of the content of this review with Ms Sameera Iqbal. Prof Nicolle Packer and Dr Lindsay Parker edited and polished the manuscript and Dr Arun Everest-Dass compiled the figures. Then, the final version was reviewed and revised by all authors.

The manuscript of the review article can be accessed via the following link: [Submitted Paper at Biochemical Society Transactions](#)

II. Verbal Presentation

Developing a 3D tissue engineering model of the brain for targeting and measuring central nervous system sugar receptors

Sameera Iqbal and ***Mina Ghanimi Fard***

I co-presented with Ms Sameera Iqbal in **BioNetwork Research Symposium 2018 “Killing it in Science”** on the 13th of April 2018, held by Centre for Nanoscale BioPhotonics (CNBP) node at Macquarie university. Ms. Iqbal first spoke for 7.5 minutes based on her own research titled as **“The effect of inflammation and pain in the expression of Polysialic acid in the central nervous system”** and I talked for an equal amount of time about my own work titled as **“Targeting sugars with bioconjugated nanodiamonds in a 3D model of human brain cancer”**.

Abstract

Glycosylation is a post-translational modification that attaches sugar receptor chains to cell surface proteins and lipids. Abnormal glycosylation is evident during multiple chronic brain pathophysiologies such as Alzheimer's, Parkinson's and Huntington's diseases and brain cancer, making sugars excellent biomarkers for selective targeting of affected cells by sugar receptors such as lectins that bind to different cell surface glycan residues. We utilised 120nm fluorescent nanodiamonds with nitrogen vacancy centres that were bio-conjugated with lectins to target sugar structures on the surface of three types of cultured central nervous system cells: astrocytes, neurons and microglia. Functionalised nanodiamonds were thus used to investigate the *in vitro* expression of sialic acid and N-acetylglucosamine (using wheat germ agglutinin), fucose (*Aleuria aurantia* lectin), and high mannose and N-acetylglucosamine (using tomato lectin) on these brain cell types. The binding of nanodiamonds to these sugars to each cell type grown in standard 2D cultures and in newly developed natural 3D brain scaffold cell growth constructs was evaluated. As glycans are a major component of the cell surface as well as of the extracellular matrix and are highly important in cell-cell interactions, our new 3D models were developed to more closely represent *in vivo* central nervous system conditions for assessing sugar expression and nanodiamond binding and uptake in neurons, astrocytes and microglia.

List of Abbreviations

2D	two-dimensional
3D	three-dimensional
AA	antibiotic antimycotic
AAL	<i>Aleuria Aurantia</i> lectin
ABC transporter	adenosine-tri-phosphate (ATP) binding cassette transporter
BBB	blood brain barrier
BSA	bovine serum albumin
BV2	mouse microglia
CFP	cyan fluorescent protein
CNS	central nervous system
CVD	chemical vapor diamond
DAPI	4',6-diamidino-2-phenylindole
DLS	dynamic light scattering
DMEM	Dulbecco's Modified Eagle's Medium
DND	detonation nanodiamond
DOX	Doxorubicin hydrochloride
FBS	fetal bovine serum
FITC	Fluorescein Isothiocyanate
GlcNAc	N-acetylglucosamine
HPHT	high-pressure hi-temperature
ECM	extracellular matrix
EDC	1-Ethyl-3-(3-dimethylaminopropyl) carbodiimide
ELISA	enzyme-linked immunosorbent assay
Em	emission
Ex	excitation
FND	fluorescent nanodiamond
FDA	Food and Drug Administration

LEL	Lycopersicon esculentum lectin (tomato lectin)
NHS	N-Hydroxysuccinimide
PC12	rat phaeochromocytoma (representing neurons)
PEG	poly-ethylen-glycol
PBS	phosphate buffer saline
QD	quantum dot
SDS	sodium dodecyl sulfate
TEM	transmission electron microscopy
U87-MG	Uppsala 87 Malignant Glioma (cancerous astrocytes)
U.S.	United States of America
UV-Vis	ultraviolet-visible spectroscopy
WGA	wheat germ agglutinin

Table of Contents

Acknowledgements	III
Declaration	V
Publications and communications arising from this thesis	VI
Abstract	VII
List of Abbreviations	VIII
Table of Contents	X
CHAPTER 1: INTRODUCTION	1
1.1 TARGETING SUGAR BIOMARKERS	1
1.2 2D AND 3D CELL CULTURING	3
1.3 NANOPARTICLE BASED DRUG DELIVERY	7
1.3.1 <i>Nanoparticle Based Drug Delivery Systems</i>	8
1.4 CNS DISEASES AND NANOPARTICLE BASED DRUG DELIVERY	10
1.5 NANODIAMOND SYNTHESIS, CHARACTERISTICS AND DRUG DELIVERY APPLICATIONS	11
1.5.1 <i>Crystallographic Defects in Nanodiamonds</i>	12
1.5.2 <i>Physicochemical Properties of the Nanodiamond Surface and Bio-conjugation Strategies</i>	14
1.6 PROJECT AIMS AND OBJECTIVES	16
CHAPTER 2: MATERIALS AND METHODS	17
2.1 NANODIAMOND BIO-CONJUGATION	17
2.1.1 <i>Raw and Bio-conjugated Fluorescent Nanodiamond Characterisation</i>	18
2.2 CELL CULTURE	19
2.2.1 <i>2D Cell Culture</i>	19
2.2.2 <i>3D Cell Culture</i>	19
2.3 LABELLING AND STAINING OF CELLS	22
2.3.1 <i>2D Samples</i>	22
2.3.2 <i>3D Samples</i>	23
2.4 DATA ANALYSIS	23
CHAPTER 3: RESULTS	25
3.1 CHARACTERISATION OF BIO-CONJUGATED NANODIAMONDS	25
3.1.1 <i>UV-Vis Absorbance and DLS</i>	25

3.1.2	<i>Transmission Electron Microscopy</i>	27
3.1.3	<i>Verification of Nanodiamond Bio-conjugation</i>	28
3.2	CNS CELL SPECIFIC TARGETING WITH LECTINS.....	29
3.2.1	<i>Qualitative Results</i>	29
3.2.2	<i>Quantitative Results</i>	36
3.3	COMPARISON OF 2D AND 3D	38
3.4	COMPARISON OF LECTIN-CONJUGATED NANODIAMONDS AND RAW- NANODIAMONDS BINDING TO CELL LINES	39
CHAPTER 4:	DISCUSSION	41
4.1	AGGREGATION OF BIO-CONJUGATED NANODIAMONDS.....	41
4.2	SPECIFICITY OF LECTINS	42
4.3	PROPERTIES OF THE 3D SCAFFOLDS.....	43
4.4	FND-LECTIN CONJUGATIONS AND THE 3D CONSTRUCTS.....	43
4.5	STAINING METHOD FOR 3D MICROSCOPY	44
4.6	CELL GROWTH PATTERNS IN THE CONSTRUCTS	45
4.7	DEVELOPING 3D BRAIN MODELS FOR SUGAR RECEPTOR TARGETING WITH BIO-CONJUGATED NANODIAMONDS AND THE FUTURE PERSPECTIVES	46
CHAPTER 5:	SUMMARY AND CONCLUSION	48
	References	XII
	Appendix	XX

Chapter 1: Introduction

1.1 Targeting Sugar Biomarkers

The surface of all eukaryotic cell membranes are coated with a layer of carbohydrates (glycans), called the glycocalyx (Figure 1), attached to transmembrane proteins and membrane lipids via the post-translational modification process of glycosylation (Brandley and Schnaar 1986, Walsh and Jefferis 2006). Binding to glycan moieties by external factors facilitates endocytosis by a ligand- receptor cell signalling process, which is the biological mechanism bacteria and viruses take advantage of in order to enter cells prior to replication (Collins and Paulson 2004). Previous literature indicates that there are glycan structure subtypes expressed more on the surface of specific cell types, making glycans suitable biomarkers and for cell type specific targeting throughout developmental stages as well as in disease and cancer (Brandley and Schnaar 1986, Yale, Nourse et al. 2018).

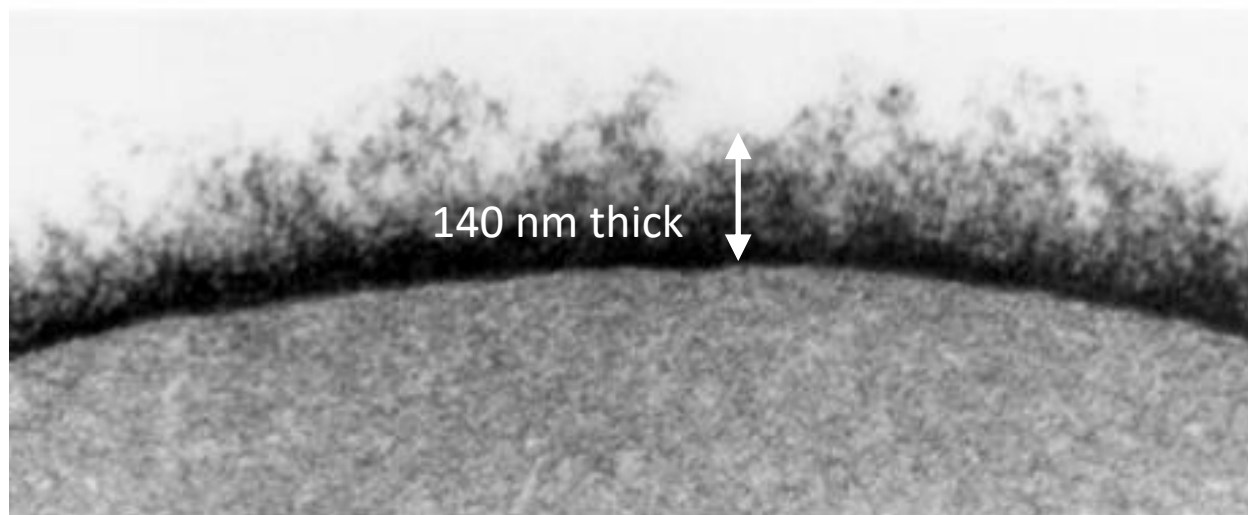


Figure1. Glycocalyx of erythrocyte. The above electron microscopy image shows a 140nm thick glycocalyx layer on top of an erythrocyte, with the diameter of oligosaccharides being about 1.2-2.5 nm. Adapted from (Roseman 2001), permission was granted for all non-commercial purposes by the journal in general.

Cancers and diseases of central nervous system (CNS) generally result in significant changes in cellular gene, protein, glycan, and/or lipid expression, giving diseased cells unique molecular signatures called biomarkers making it possible to differentiate them from healthy cells (Srinivas, Kramer et al. 2001). Some of the current methods used for the

discovery of these biomarkers are microarrays, surface-enhanced laser desorption/ionization, isotope-coating affinity tag, protein arrays, tissue microarrays (Hewitt 2004), liquid chromatography and mass spectrometry (Liao, Wu et al. 2004). Although biomarker discovery studies began as early as the 1960s (eg. carcinoembryonic antigen), only a limited number of them have resulted in clinical application outcomes to date, potentially due to targeting specificity and sensitivity issues (Diamandis 2012).

Glycan biomarker discovery has attracted much attention in recent years. Glycans modify the surface of around 50% of all human proteins and changes to glycan biosynthesis during diseases can be far more obvious than for protein molecules (Adamczyk, Tharmalingam et al. 2012). Glycoproteins are in general classified into two main groups: N-linked glycans (N-glycans) and O-linked glycans (O-glycans); which indicates whether they bind to the nitrogen atom of an asparagine residue on a protein, or the oxygen atom of a serine or threonine of disulfide bond on a protein (Ajit Varki and Jeffrey D Esko 2015-2017). The core sugar motif of all N-glycans, known as chitobiose core, is consisted of two N-acetylglucosamine (GlcNAc) and 3 mannose monomers. Three structural subtypes of N-glycans include: (1) high mannose, that is made of the core with only mannose residues; (2) complex, in which “antennae” are attached to the core; and (3) hybrid, which is a combination of the other two types (Ajit Varki and Jeffrey D Esko 2015-2017). However, the core structure of O-glycans are more varied and shorter structures than N-glycans, core1 to core4 are the most studied in mammalian O-glycans (Chik, Zhou et al. 2014).

For targeting sugars as biomarkers, lectins and antibodies with binding sites that are exclusive to specific kind of sugars with high affinity can stimulate endocytosis thus are particularly useful (De Mejia and Prisecaru 2005, Sharon 2007, Gabius, Andre et al. 2011).

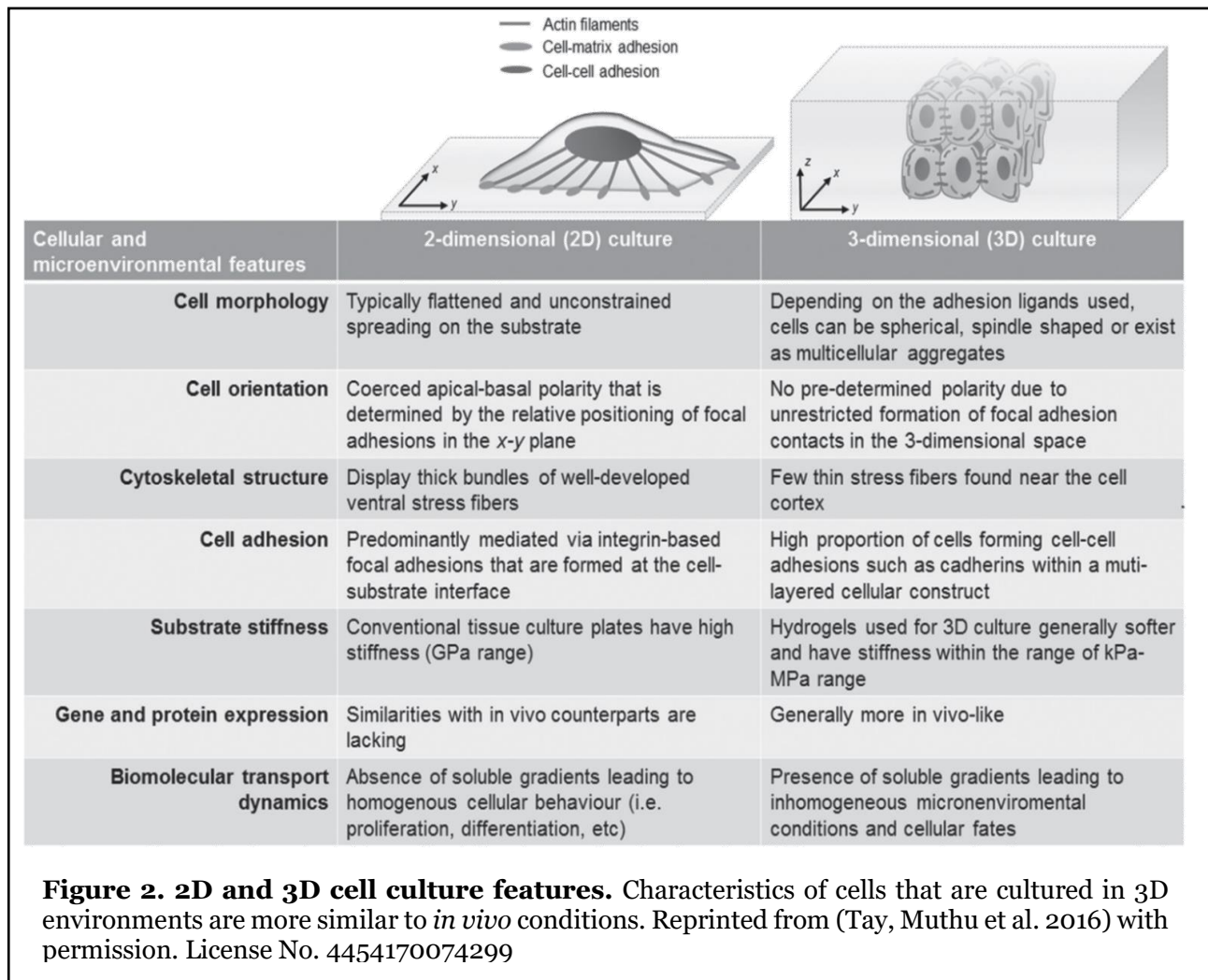
For example, modifications to the N-glycans of breast cancer cell membranes were profiled using DNA sequencer-assisted fluorophore-assisted carbohydrate electrophoresis to identify biomarkers across 8 different cell lines (Liu, Nie et al. 2013). Additionally, in 2014 it was demonstrated that 5 colorectal cancer cell lines could be distinguished from each other by identification of their surface N-glycans, which were grouped into bisecting, fucosylated, sialylated, paucimannosidic and Lewis-type (Chik, Zhou et al. 2014). Fucose containing cell surface N-glycans are upregulated in glioblastoma multiforme as detected by the lectin *Ulex europaeus* agglutinin I (VanderMeulen, Prasad et al. 1994) or HPLC columns with fluorescent detection (Tsuchiya, Yamanaka et al. 2005). Fucose has also been identified by others as a potential marker for cancerous cells, including oral (Kumar, Saxena et al. 2015), head and neck (Shetty, Bhandary et al. 2013), liver, pancreatic and prostate (Adamczyk,

Tharmalingam et al. 2012) cancers. The fungal derived fucose-specific lectin *Aleuria aurantia* Lectin AAL has previously been used with lectin-antibody ELISA kit and Western blotting to target fucose on the surface of liver cancer cells for diagnosis purposes (Miyoshi, Moriwaki et al. 2012, Norton, Comunale et al. 2016), indicating that fucose glycan structures identified on human glioblastoma multiforme cells could potentially be targeted in a similar way (Olausson, Tibell et al. 2008). Also in this type of glioblastoma, an increase in polysialic acid is observed (Amoureux, Coulibaly et al. 2010), which can be targeted by wheat germ agglutinin (WGA), similar to any sialic acid residue (Lenman, Liaci et al. 2018). Sialic acids are expressed abundantly on the surface of neurons (Schnaar, Gerardy-Schahn et al. 2014), so they can also be targeted by WGA. Another interesting lectin that has previously been used for targeting a specific type of brain cell (microglia) is the lectin from tomato (*Lycopersicon esculentum* lectin, or LEL), which has shown specificity for N-acetylglucosamine (GlcNAc) (Wohl, Schmeer et al. 2011). However, some lectins such as WGA and LEL have more than one specific binding site for sugars. For example, GlcNAc is also detected by WGA, demonstrating that this lectin has two different specificities, and also that both WGA and LEL can recognise GlcNAc on the surface of the cells. It is also worth mentioning that LEL can also bind to poly N-acetyl lactosamine (Villacampa, Almolda et al. 2013) and high mannose N-glycan structures, which are also beneficial for targeting microglia (Oguri 2005).

1.2 2D and 3D Cell Culturing

Regardless of the quality of results, much of the published literature on nanoparticle-based drug delivery has been conducted in 2D cell cultures, (Bielecka, Maliszewska-Olejniczak et al. 2017, Duval, Grover et al. 2017, Fang and Eglen 2017). It is normal that many cell types develop a monolayer at the bottom of plastic flasks or glass coverslips due to the stiffness of these substrates. This stiffness consequently alters cellular interactions between cells and with external factors such as nanoparticles therefore results are not highly realistic or comparable to *in vivo* conditions in humans and animal models (Bielecka, Maliszewska-Olejniczak et al. 2017, Duval, Grover et al. 2017, Fang and Eglen 2017). This may account for some of the reasons that nanoparticle drug delivery experiments do not translate well into clinically approved systems (Souza and C Ferreira 2016, Bielecka, Maliszewska-Olejniczak et al. 2017, Duval, Grover et al. 2017, Fang and Eglen 2017). Major differences in several factors including: cell morphology, cell orientation, cytoskeletal structure, cell adhesion, substrate stiffness, gene and protein expression, as well as biomolecular transport dynamics have been described in 2D versus 3D cultures (Figure 2). To overcome this inaccuracy, 3D cell culturing systems with more well developed extracellular matrix environments made

through spheroids, droplets, and natural or artificial scaffolds have emerged as far better models of natural cell conditions (Duval, Grover et al. 2017), especially for testing in clinical applications (Koch, Munster et al. 2012).



Topological, chemical and physical properties of the extracellular matrix lead to production of signals for versatile cellular functions (Scadden 2006, Underhill and Bhatia 2007, Tyrrell, Shen et al. 2010). For example, in 2D cultures fibronectin or collagen can be used to imitate natural functions of the extracellular matrix (Chaubey, Ross et al. 2008) although the usage of collagen in 3D cell cultures is instead used for enhancing control on individual properties and lowering the impact of degradation (Duval, Grover et al. 2017). Cells grown on collagen in 2D versus 3D thus show different behaviours due to their chemical and mechanical conditions (Figure 3). The impact of 2D and 3D cell cultures on the expression of genes, proliferation and differentiation of cells has also been extensively investigated, showing that collagen coated cells in 2D culture differentiated faster than those in 3D, overall proliferation of all cell lines in 2D culture were higher than cell lines cultured in 3D scaffolds

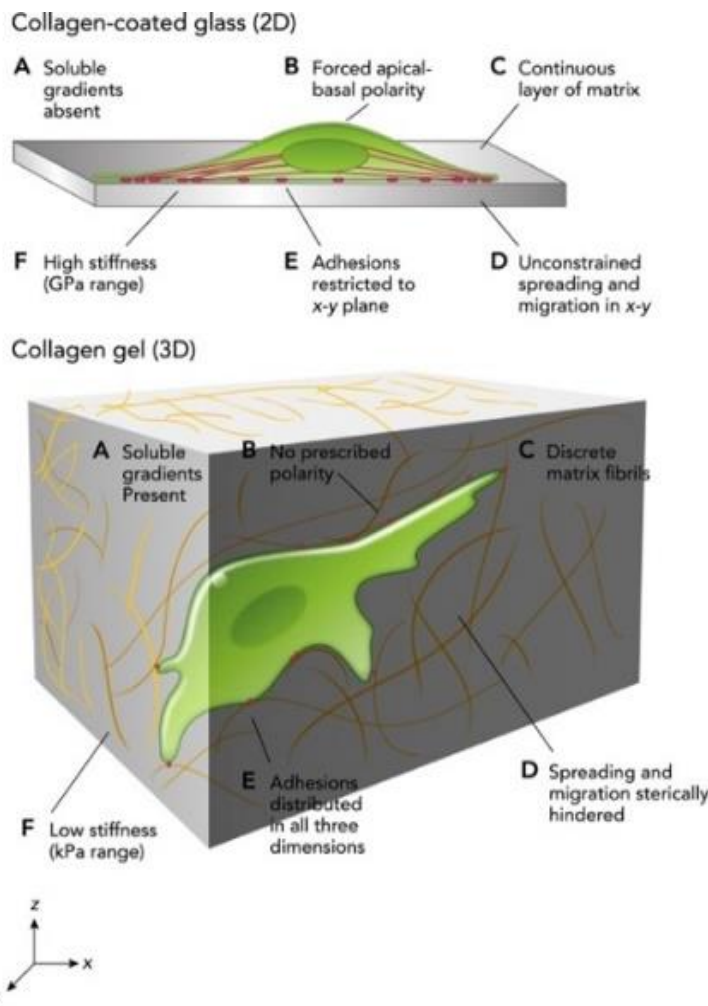


Figure 3. 2D Versus 3D cell culture. Differences of 2D and 3D collagen gel cell cultures in presence or absence of ECM. Reprinted with permission from (Duval, Grover et al. 2017). License No. 4324790253750

(with some exceptions) and the genes of the cells in 2D and 3D cultures express different phenotypes from each other, consequently causing differences in the stiffness and quantity of cytoskeletal and extracellular matrix proteins (Chitcholtan, Asselin et al. 2013, Pineda, Nerem et al. 2013, Mabry, Payne et al. 2016). The migration of cells is also drastically changed in different dimensional cultures, and this is an important factor especially in studying the motion and migration of metastatic cancer cells (Scadden

2006, Bott, Upton et al. 2010, Gjorevski, Piotrowski et al. 2015). The difference in the migration of cells in 2D and 3D cultures could be due to the positioning of the cells, as in 3D scaffolds the cells are surrounded by tissue walls that may prevent them from movements, while in 2D they can freely move around (Grinnell 2003, Yoshii, Waki et al. 2011). In spheroid 3D cultures, cells aggregate to form a spherical shape, which may not necessarily be a perfect sphere, but are referred to as spheroids, mammosphere, micromass, microfabricated tissues or aggregates (Fennema, Rivron et al. 2013). There are several innovative techniques available for this, namely embryoid bodies, microchips, collagen gels, microfluidics and hanging drop cultures (Torisawa, Takagi et al. 2007, Tung, Hsiao et al. 2011, Pineda, Nerem et al. 2013). Some of these methods use a non-natural environment such as silicon triangular arrays or micro rings to produce cell aggregates and each method results in different cell interaction models, indicating that the form and material of

environmental tissues have an important impact on intracellular and extracellular interactions (Duval, Grover et al. 2017). For example, in a comparison of 3D cultures within collagen gel and non-tissue culture dishes, and despite similar morphology of the developed spheroids, their genetic expression levels greatly varied after 12 days (Pineda, Nerem et al. 2013).

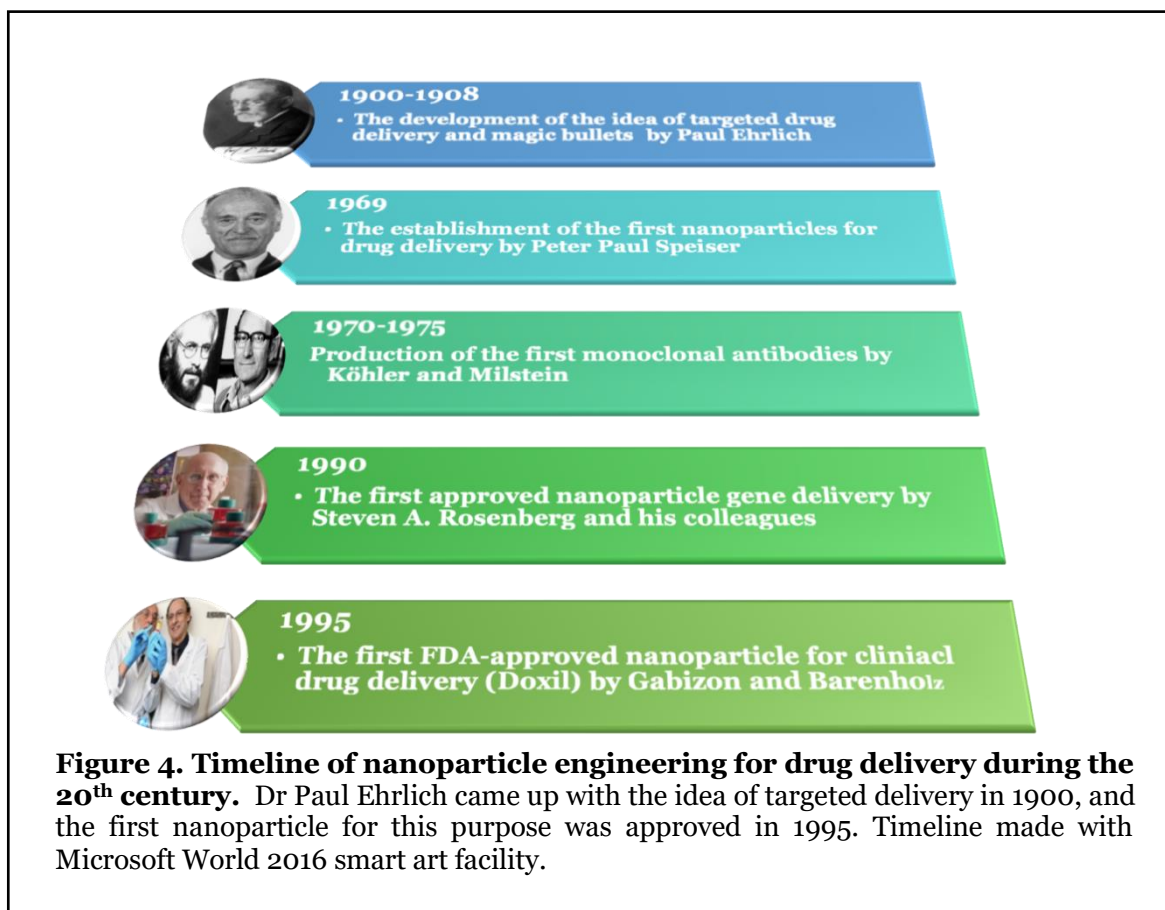
Various 3D scaffolds have therefore been engineered for entrapping cells into biomechanical and biochemical environments to provide more realistic results (Cukierman, Pankov et al. 2001). Biopolymer 3D scaffolds can be produced from either cellular tissue such as animal cells or from non-cellular compounds, with substrates such as alginate, chitosan, chondroitin sulfate, hyaluronic acid, collagen and gelatine being the most popular biopolymers used (Duval, Grover et al. 2017). Hydrogels are also very popular in tissue engineering, which are polar polymers with crosslinked networks that inflate in water but are also water-insoluble, making them suitable for biomedical applications such as drug delivery (Zhu and Marchant 2011). Natural, synthetic or hybrid hydrogels are ideal as 3D scaffolds because their structure is similar to natural tissues, they are biocompatible and allow for transportation of nutrients, water and oxygen into the seeded cells inside them (Zhu and Marchant 2011). All classes of hydrogels are designed in a way to be biodegradable for production of cell matrices, but this characteristic is also a drawback, because over time by degradation they lose their necessary elasticity for cell growth and the biochemical elements (Slaughter, Khurshid et al. 2009). Successful non-biodegradable cell sheet scaffolds have also been developed by layering several natural tissue layers and applied into cornea, heart, liver and kidney of live rats with a survival time of 3 months (Shimizu, Yamato et al. 2003), confirming that biodegradable materials are not necessary for 3D cell cultures (Duval, Grover et al. 2017).

Tumour tissue engineering of natural decellularized organ scaffolds is another alternative approach of 3D cell culturing (Eggleton, Palomba et al. 2015). Decellularization of organs for obtaining an acellular unit of extracellular matrix has been used for different therapeutic purposes since 1910 (Solez, Fung et al. 2018), usually for regeneration of tissues and replacing new cells in the body (Badylak 2004). However, in recent years this method has widely been utilised for studies on overcoming the issue of organ transplantation failures by patient bodies (Yu, Alkhawaji et al. 2016, Remuzzi, Figliuzzi et al. 2017, Guruswamy Damodaran and Vermette 2018). 3D extracellular matrix scaffolds are also being tested to use for obtaining more realistic results in the regeneration of tumour cells and experimental drug delivery in tissues (Anna Guller and Yi Qian 2015). These biocompatible acellular tissue scaffolds can be produced by detergent-based processing using perfusion or

immersion-agitation of various organs from animal bodies such as liver, lung, heart, kidney and ureter (Eggleton, Palomba et al. 2015). The scaffolds have successfully allowed production of sustainable tissue engineered 3D tumour cells and show promise for oncologic studies in the future (Eggleton, Palomba et al. 2015).

1.3 Nanoparticle Based Drug Delivery

Nanomaterials were used in decorative objects as early as the 4th century, for example gold and silver nanoparticles were used in antique Roman dichroic glass cups that make their olive green colour turn into ruby by the change of light direction towards the glass (Krukemeyer, Krenn et al. 2015). However, it was not until the early 20th century that innovations in chemistry, physics and pharmaceuticals, as well as the development of advanced microscopy and imaging devices, led to the idea and first attempts of targeted drug delivery via nanoparticles (Krukemeyer, Krenn et al. 2015).



The Nobel prize winner Doctor Paul Ehrlich came up with the targeted drug delivery initiative using inspiration from his past tissue staining experience and research into antibodies (Schwartz 2004). His concepts in 1908 suggested that specific drugs could be fired at targeted microbes to kill them all with only one shot and without harming the healthy tissues of patient's body, so he named the system "magic bullets" (Datta, Krishnan et al.

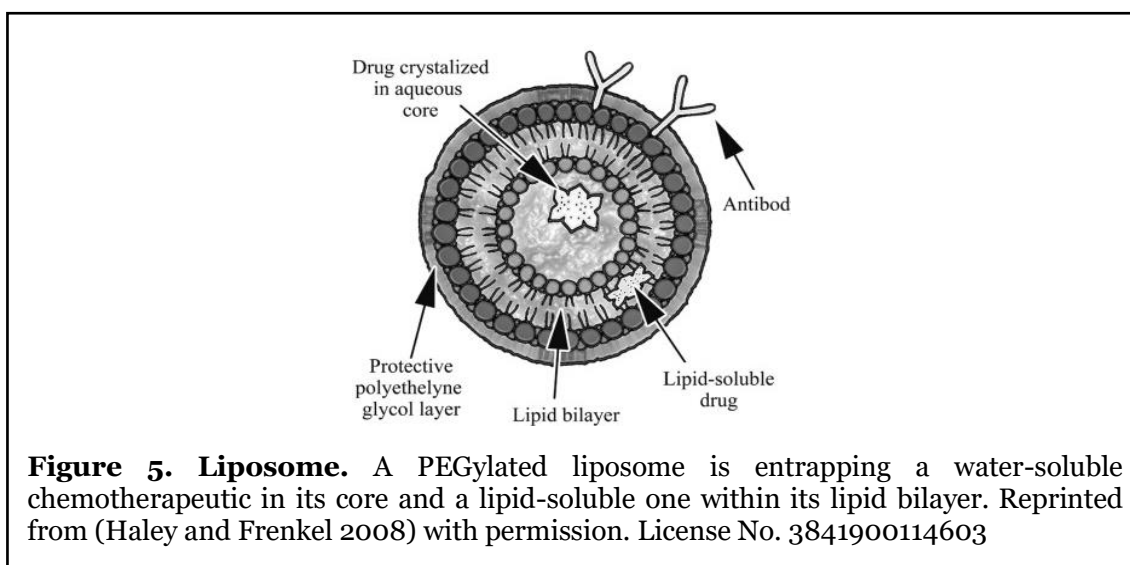
2016). Although he did not achieve his concept using nanoparticles, he was able to invent a drug to treat syphilis called “Salvarsan” through his research into “magic bullets” (Strebhardt and Ullrich 2008).

Professor Peter Paul Speiser furthermore advanced this field in the 1950s and 1960s, establishing the very first nanoparticles for the purpose of drug delivery in 1969 (Kreuter 2007). His ultimate aim was to deliver vaccines using polymerised nanoparticles he developed in order to reduce the number of injections from multiple repetitions to only once by achieving high immunity with the sustained release of antibodies (Kreuter 2007). One of Speiser’s students, Gerd Birrenbach, designed the micelle polymerisation process to encapsulate drugs inside polyacrylic beads, however he could not continue this project due to the toxicity of the acrylamide monomers and the required high amount of organic materials (Kreuter 2007). Speiser’s other graduate students and collaborators then continued this research to improve drug delivery by nanoparticles (Kreuter 2007).

In the 1970s, Georges J. F. Köhler and César Milstein won the Nobel prize for production of monoclonal antibodies (Freysd’ottir 2000) from continuous culture of fused cells (Köhler and Milstein 1975). This was the beginning of a new era for several researchers to investigate various nanocarriers for drug delivery and modification of their surface using diverse chemical and physical functionalisation methods (Krukemeyer, Krenn et al. 2015). Subsequently, at the beginning of 1990s gene delivery via nanoparticles and endocytosis was achieved with the help of antibodies (Rosenberg, Aebersold et al. 1990, Kreuter 2007) and in 1995 Doxil (liposomal doxorubicin) was approved by the U.S. Food and Drug Administration (FDA) for clinical application (Barenholz 2012) (Figure4). There is a large variety of nanoparticle-based drug delivery systems available today, including but not restricted to liposomes, micelles, dendrimers and particle chemical conjugation such as to quantum dots and nanodiamonds (Mudshinge, Deore et al. 2011). Each of these delivery routes is engineered and specified for a list of advantages over the others but carrying its own drawbacks.

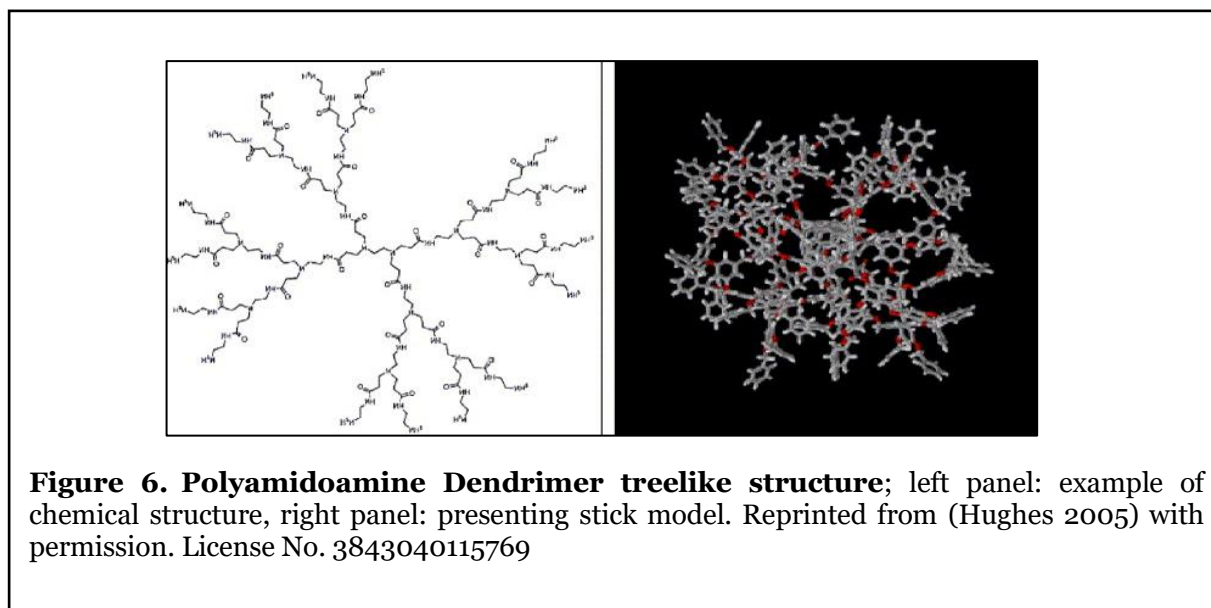
1.3.1 Nanoparticle Based Drug Delivery Systems

Liposomes (Figure 5) are nanoscale closed space circular vesicles with aquatic cores and with either multiple or one phospholipid bilayer that vary in size between 20 nanometres to a few micrometres (Coune 1988). Liposomes have the ability to entrap both lipophilic drugs and hydrophilic therapeutics, as shown in Figure 5, to reduce the toxicity of drugs towards healthy cells (Yu, Tai et al. 2010).



However, drug delivery via liposomes can lead to complement activation-related pseudo-allergy because of a natural immune response in humans (Sercombe, Veerati et al. 2015, Lamichhane, Udayakumar et al. 2018). Moreover, macrophages from the lymph nodes, spleen and liver eliminate regular liposomes from blood circulation quickly (Torchilin 2005). To overcome this issue for drug delivery applications, liposomes are coated with polyethylene glycol (PEG) hydrophilic polymers that increase their circulation lifetime (Nag and Awasthi 2013).

Like liposomes, micelles are amphiphilic vesicles but consist of only a monolayer of surfactant molecules such as detergents (Tyrrell, Shen et al. 2010). The hydrophobic tails of micelles gather at the nonpolar core of these vesicles, which is suitable for encapsulation of less aqueous soluble drugs (Tyrrell, Shen et al. 2010). Micelles are usually between 2-20 nm,



but their size after loading with drugs is bigger than 5.5 nm and will not be cleared well by kidneys, which increases their circulation half-life, and reduces their accumulation in

kidneys, making them more suitable for drug delivery (Ahmad, Shah et al. 2014). Similar to liposomes micelles are commonly PEGylated for increasing their circulation longevity (Zhang, Huang et al. 2014).

Dendrimers (Figure 6) are snowflake like in shape, globular and multi-branched with a flower-like core and a size of about 20 nm (Mudshinge, Deore et al. 2011). Dendrimers are made of different chemicals that can be hydrophobic or hydrophilic, but the ones that are made of polyamidoamine (PAMAM) are the most utilised ones for drug delivery (Palmerston Mendes, Pan et al. 2017). PAMAM dendrimers are biocompatible, polar and are not filtered by macrophages, thus making them more suitable for the purpose of drug delivery (Palmerston Mendes, Pan et al. 2017). However, their strong positive charge disrupts negatively charged cell membranes and leads to cell lysis, hence these nanoparticles are classified as toxic (Palmerston Mendes, Pan et al. 2017). Dendrimers are also generally PEGylated to modify their surface and increase their circulation time, plus reducing their cytotoxicity (Palmerston Mendes, Pan et al. 2017).

Fluorescent semiconductor nanocrystals with more efficient characteristics than other microscopy fluorophores, such as quantum dots, can also be utilised for delivering drugs to targeted cells (Qi and Gao 2008). The ability of quantum dots to emit fluorescence following light excitation under the microscope, enabling the targeted delivery of therapeutics to be *traceable*, makes them ideal for utilisation in drug delivery applications although their cytotoxicity remains a big issue and limits their usage to *in vitro* and small animals experiments (Qi and Gao 2008). Other more recently utilised fluorescent nanocrystals with low cytotoxicity such as nanodiamonds and nanorubies have also shown promise in drug delivery applications in animal models (Zhu, Li et al. 2012, van der Laan, Hasani et al. 2018) and the ability for continuous tracking/imaging even at the single receptor level is superior to quantum dots as they are photostable and do not blink (Sreenivasan, Wan Razali et al. 2017).

1.4 CNS Diseases and Nanoparticle Based Drug Delivery

The central nervous system consists of several different cell types, including neurons and glial cells. Glial cells support the neurons, and include: astrocytes, microglial cells, oligodendrocytes and ependymals (Jäkel and Dimou 2017). The blood brain barrier (BBB) controls trafficking of molecules to the brain cells and blocks the entrance of the medicine into the cells (Jain 2007). In most cases even after the entry of common therapeutics, BBB effluxes them via ABC (ATP binding cassette) transporter proteins (Xue and Liang 2012). Various nanoparticles are presently under investigation as emerging carriers for

transportation of medicine across the BBB by targeting the surface cell trafficking molecules and initiation of endocytosis (Jain 2007).

To target and deliver drugs into cancer cells via nanocarriers, either active or passive targeting methods are exploited. Passive targeting is feasible due to the enhanced permeability and retention (EPR) effect of tumours (Iyer, Khaled et al. 2006). When cancer tumours enter the angiogenesis stage, they start to form blood vessels around them, leading to generation of a leaky blood environment that is highly permeable to nanoscale molecules (Iyer, Khaled et al. 2006). Such specificity makes it possible for nanoparticles to passively target tumours by entering from the permeable bloody surface into cancerous cells and remain there (Iyer, Khaled et al. 2006). Although this method has been approved and used for several years, it has faced many challenges due to differences in particle size, charge, shapes (Bertrand, Wu et al. 2014) and the location of different tumours, as well as characteristics of different drugs, nanoparticles and tissues (Prabhakar, Maeda et al. 2013). More than 95% of drugs that are delivered with passive targeting methods also accumulate in other organs such as liver, lung and spleen, because they move through the blood circulation and do not possess any specific binding moieties to match the receptors of targeted cells to enter them (Bae and Park 2011). Active targeting is more efficient, as it includes ligand-receptor interactions on the surface of targeted cells to enable endocytosis of desired drugs (Yu, Tai et al. 2010). Glioblastoma multiforme is the most aggressive cancer of the CNS, corresponding to malignant astrocytes, (Urbanska, Sokolowska et al. 2014) and therefore nanoparticle delivery to glioblastoma astrocytes has been well studied. For example, very recently cisplatin-gold-nanoparticle conjugates were successfully delivered to glioblastoma cells using focused ultrasound to magnetically guide them via resonance (Coluccia, Figueiredo et al. 2018). Another recent study found a promising method by exploitation of small lipid nanoparticle charge for delivery of chemotherapeutics to glioblastomas (Zhang, Xiao et al. 2018). A third recent example demonstrated effective delivery of drugs to glioblastoma via upconversion nanoparticles (Tsai, Vijayaraghavan et al. 2018).

1.5 Nanodiamond Synthesis, Characteristics and Drug Delivery Applications

Fluorescent nanodiamonds (FNDs) are nanoscale diamond crystals with a point defect in their atomic lattice (Mochalin, Shenderova et al. 2011). FNDs are a member of the carbon nanoparticle family with a size generally ranging from 1 nm to 150 nm (Chow, Zhang et al. 2011). FNDs have consistently been reported as non-toxic, photostable, biocompatible,

water dispersible and extremely pH and temperature resistant nanoparticles (Huang, Pierstorff et al. 2007, Li, Zhu et al. 2010, Zhu, Li et al. 2012, Kaur and Badea 2013, Zhang, Niu et al. 2014, Chen and Zhang 2017, Roy, Drozd et al. 2018). They also possess properties such as high adsorption capacity and large surface area (Mochalin, Shenderova et al. 2011), which makes them ideal for surface binding (Zhu, Li et al. 2012) and additionally they are rigid and durable like natural diamonds (Chen and Zhang 2017).

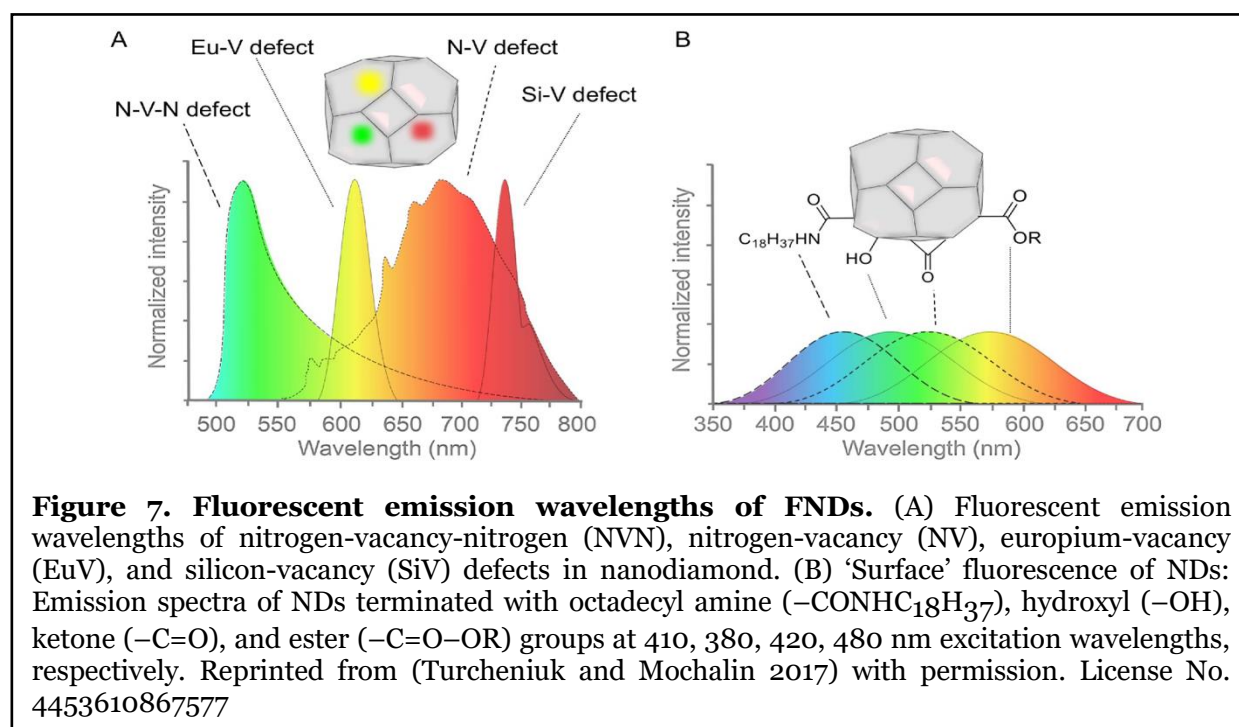
Nanodiamond synthesis occurs primarily in one of three ways: (1) high-pressure-high-temperature (HPHT) treatment; (2) detonation (DNDs); (3) chemical vapour deposition (CVD) (Holt 2007). HPHT nanodiamonds are manufactured within a machine at ~1500-1600°C with a pressure of ~5-10 GPa, which turns graphite carbon into its crystal structure or diamonds, prior to being ground and milled to a smaller size (Pal'yanov, Sokol et al. 2002). DNDs as their name suggests, are made by an explosion of materials such as trinitrotoluene (TNT) with research department explosive (RDX) or hexogen in a chamber, that provide a shock wave compression to NDs with almost 3 times higher pressure and temperature than the HPHT nanodiamond production (Dolmatov 2001). This subsequently results in nanodiamonds of 4-5 nm size, almost 20 times smaller than HPHT nanodiamonds (Tong, Liu et al. 2014). The CVD procedure involves hydrogen and hydrocarbon gases such as methane. In this method the gases are controlled, and temperature and pressure are increased gradually, starting from 1000-2000K and about 27 KPa, with nanodiamond crystals being formed at ~800°C on the surface of a desired substrate (Shenderova and McGuire 2015). This method is not as cost effective as HPHT treatment or detonation treatment but is gaining interest because of the chemical deposition controllability (Shenderova and McGuire 2015).

1.5.1 Crystallographic Defects in Nanodiamonds

Nanodiamonds, like other crystals, may be produced with two types of defects: intrinsic and extrinsic. Intrinsic defects are a result of the misplacement or absence of one or more carbon atoms in their atomic lattice structure, known as vacancy, or broken bonds between carbon atoms, called dislocation. Whereas, an extrinsic defect is known as the presence of one or more atoms of another element (Figure 7), such as nitrogen, silicon, boron, nickel, chromium, germanium, oxygen, hydrogen, lithium, helium, titanium, zinc, arsenic, silver, phosphorus, neon, tungsten, thallium or silicon in the nanodiamond atomic lattice structure that causes impurity (Walker 1979, Collins 2002, Iakoubovskii and Collins 2004, Vlasov, Barnard et al. 2009, Iwasaki, Ishibashi et al. 2015). These impurities provide unique optical properties to nanodiamonds such as fluorescent light emission in response to excitation by

a high energy laser. Nearly all nanodiamond based research for biological targeting has been conducted using nitrogen vacancy (NV) diamonds (Yu, Kang et al. 2005, Huang, Pierstorff et al. 2007, Vijayanthimala and Chang 2009, Vlasov, Barnard et al. 2009, Xing and Dai 2009, Barras, Szunerits et al. 2010, Li, Zhu et al. 2010, Wrachtrup 2010, Chow, Zhang et al. 2011, Kaur and Badea 2013, Zhang, Niu et al. 2014, Bradac, Say et al. 2016, Khalid, Mitropoulos et al. 2016) although silicon vacancy (SiV) nanodiamonds (Merson, Castelletto et al. 2013) have recently been utilised as well for bio-imaging applications with success (Shimoni, Bray et al. 2017).

When excited with 532nm laser light (green spectrum), point defects of nitrogen vacancy centres in the atomic lattice of nanodiamonds emit in the near infrared wavelength (700-800nm) (Reineck, Lau et al. 2017). Compared to many other organic fluorescent dyes and carbon dots that lose their brightness after excitation by light (Reineck, Lau et al. 2017, Cordina, Sayyadi et al. 2018), nanodiamonds are resistant to photobleaching even after hours of light excitation (Yu, Kang et al. 2005). The high photostability of nanodiamonds is also superior to quantum dots due to: (1) the excited state in quantum dots being spread all over its volume, while in nanodiamonds the excited state is localised at the centre where the defect atom is located; (2) the energy level of the NV centre and that of the host diamond are detached from one another, so photoelectrons stay surrounded by the carbon atoms within the vacancy centre and even the highest power laser irradiation cannot remove them (Wrachtrup 2010).



1.5.2 Physicochemical Properties of the Nanodiamond Surface and Bio-conjugation Strategies

In contrast with conventional diamonds, FNDs are hydrophilic, and have high colloidal stability in water (Kaur and Badea 2013) due to their large surface area in relation to volume and a surface charge that is not zero (Bradac, Say et al. 2016). FNDs can tolerate extreme pH and temperatures, as well as room temperature and laboratory conditions, as their unique crystal structure includes strong covalent carbon bonds in a highly ordered atomic lattice providing a controllable chemistry and high binding specificity (Bradac, Say et al. 2016). For the bio-conjugation of nanodiamonds with carbodiimide chemistry, strong acids can be employed for preparation of carboxylated surfaces on them, and organosilanes and long chain alcohols can help to functionalise hydroxyl groups (Bradac, Say et al. 2016) prior to the essential functionalisation of their surface in order to conjugate targeting and/or drug molecules (Vaijayanthimala and Chang 2009, Kaur and Badea 2013). CVD nanodiamonds, negatively charged HPHT nanodiamonds and positively charged DNDs are all suitable for drug delivery purposes (Robert Lam 2009, Lin, Lin et al. 2015).

Polyethylene glycol (PEG) is widely used for the surface modification of different nanocarriers in order to reduce toxicity or increase water solubility and circulation half-life (Xing and Dai 2009). Carboxy- and amino- PEG Spacer arms have been used to decrease non-specific binding for example in quantum dots (QD) in 2008 (Liu, Howarth et al. 2008). While nanodiamonds do not require a PEGylated surface to possess the above advantageous properties, the molecules to be bound to FND (ligand protein or drug) can benefit from a hydrophilic PEG spacer arm in order to enhance their stability in liquid solvents (Sperling and Parak 2010).

Nanodiamonds have been tested for biocompatibility *in vitro* and *in vivo* and show little or no cytotoxicity, in contrast to quantum dots and carbon nanotubes (Mochalin, Shenderova et al. 2011, Zhu, Li et al. 2012). For instance, carbon nanotubes are usually contaminated with catalyst metal impurities such as transitional metals (Fe, Y, Ni, Co and Mo) or amorphous carbon, during their synthesis or purification procedures these toxic chemicals can be released into human body by single layer nanotubes (Liu, Gurel et al. 2007, Liu, Zhao et al. 2013). However, the inert nature of nanodiamonds does not allow them to release toxic chemicals when they are exposed to harsh environments (Chen and Zhang 2017) as they do not have free electrons on their bulk structure despite the fact that their surface structure that can have univalent electrons (Kaur and Badea 2013). Nanodiamonds are therefore ideal to be used for the targeted delivery of modern therapeutic medicines whilst also carrying out

bio-imaging in order to assess the localisation of drugs and cellular uptake (Chen and Zhang 2017). They have been used to track delivery of drugs such as anti Human Immunodeficiency Virus Type 1 (HIV-1) across the blood brain barrier (Roy, Drozd et al. 2018) and have been used as nanocarriers of various drugs for cancer treatment during recent years (Kaur and Badea 2013).

The first successful study of nanodiamond-based drug delivery to cancer cells took place in 2007, when nanodiamonds were loaded with an apoptosis-inducing anticancer medicine, doxorubicin hydrochloride (DOX) to enhance the bioavailability and efficacy of DOX (Huang, Pierstorff et al. 2007). Four years later, it was explained theoretically (Figure 8, A) and practically (Figure 8, B and C) that nanodiamonds not only overcome efflux, but also increase apoptosis and inhibition of growth in breast and liver cancer cells while loaded with DOX (Chow, Zhang et al. 2011, Merkel and DeSimone 2011). Other anti-cancer medicines have also been loaded on nanodiamonds to effectively target metastatic gastrointestinal cancer cells *in vitro* (Zhang, Niu et al. 2014) and nanodiamonds have been successfully

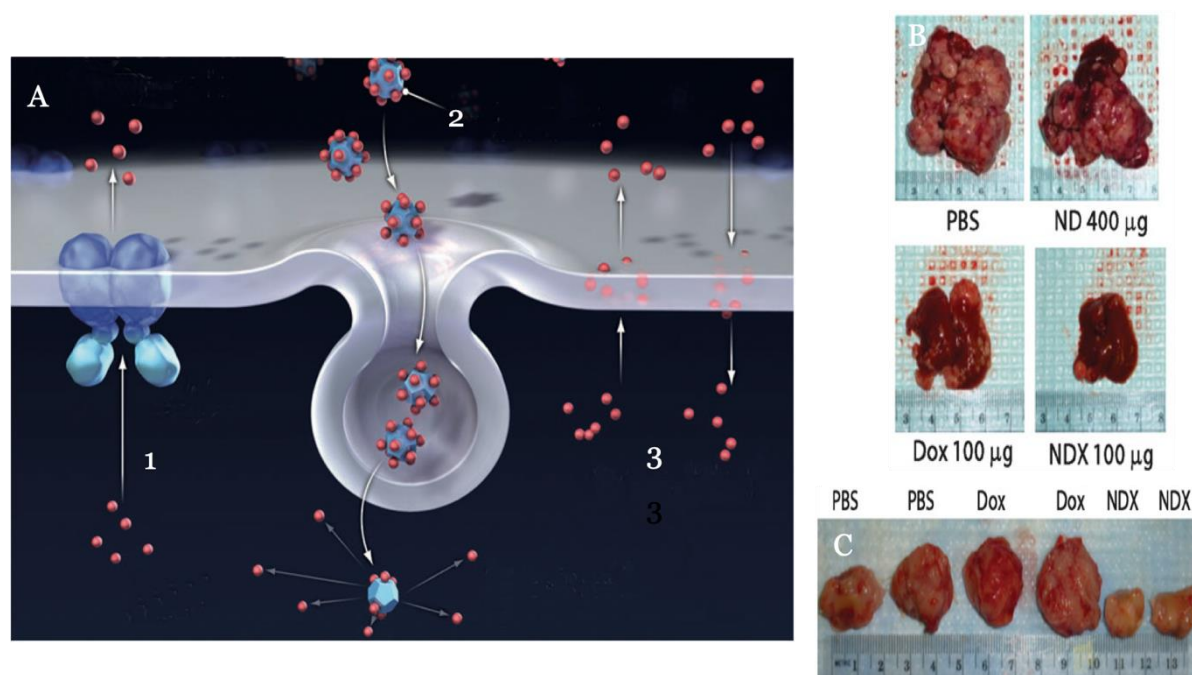


Figure 8. Drug delivery by nanodiamonds. **A.** Proposed mechanism of Nanodiamond-drug uptake by efflux-transporter expressing cells: **1.** ABC transporter proteins on the membrane efflux the drug molecules after uptake. **2.** Endocytosis and remaining of the drug-conjugated nanodiamond inside the cell. **3.** Passive diffusion of therapeutics via the cell membrane and the easy removal of it from the cell. Adapted from (Merkel and DeSimone 2011) . **B and C.** Images of liver and breast cancer tumours of mice respectively, after treatment by DOX-ND (NDX) conjugates compared to controls of free DOX, free NDs and no treatment. The NDX treated tumour is significantly smaller than the other tumours, confirming that drug conjugated nanodiamonds can reduce the size of tumours more efficiently than free chemotherapeutics as proposed in image A. Adapted from (Chow, Zhang et al. 2011) with permission. License No. 4455160666912

targeted to cells whilst overcoming their efflux (Man, Kim et al. 2014). Despite the high popularity of nanodiamonds as drug delivery agents (Chen and Zhang 2017), the medicines may also affect healthy cells if they are not designed to target diseased cells only, for instance DOX causes heart failure in cancer patients (Wang, Konorev et al. 2004). Hence, selective targeting of diseased cells in exclusion of healthy cells becomes an important and emerging subject of study.

1.6 Project Aims and Objectives

The general aims of this project were:

- 1) To achieve an alternative to antibody selective targeting of the different cell types in the brain by using lectins to target cell surface sugars that are known to alter in different diseases.
- 2) To use lectin-conjugated nanodiamonds as delivery agents and imaging probes, due to the excellent fluorescence, non-bleaching nature and biocompatibility of nanodiamonds.
- 3) To develop a 3D cellular growth platform to study cell surface targeting using lectin-conjugated nanodiamonds in a more natural cell environment.

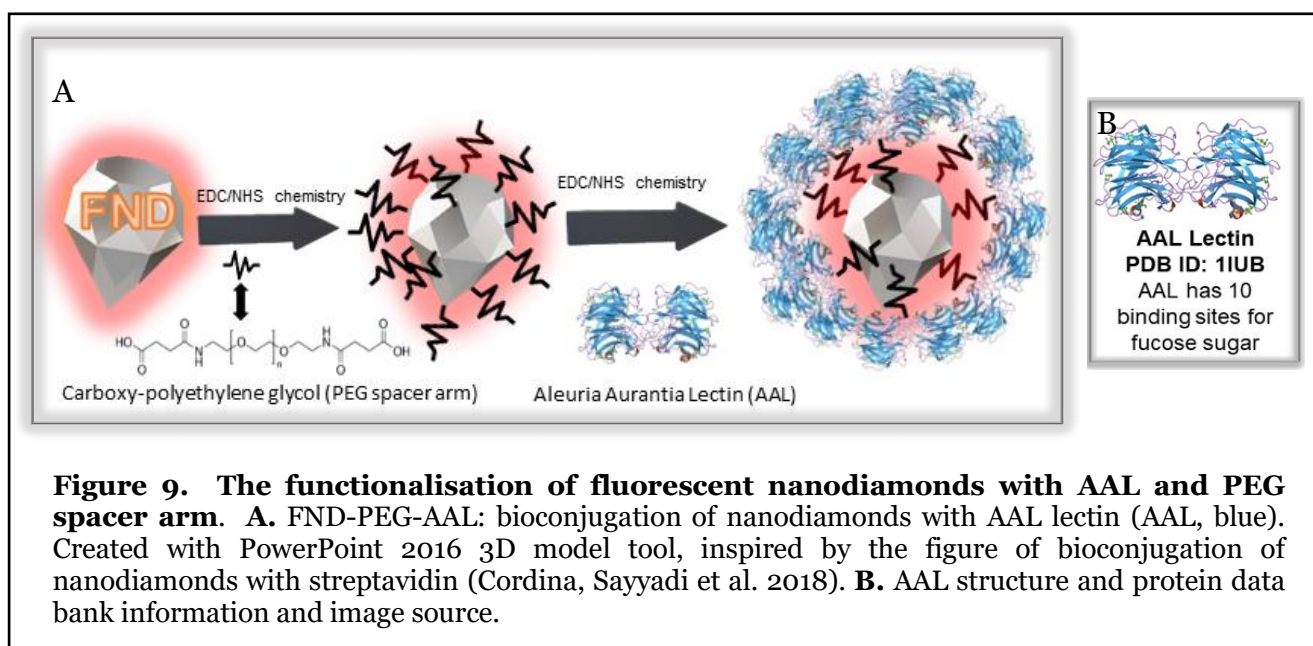
The more specific objectives of this study included:

- 1) To target astrocytes, neurons and microglia cells selectively by using AAL, WGA and LEL lectins, to investigate whether the profile of fucose, sialic acid, and GlcNAc expressed on their surfaces is different in one compared to the others;
and correspondingly
- 2) To use these nanodiamond conjugated lectins to compare the cell surface glycosylation profile of the brain cells grown in a newly developed 3D growth scaffold model with cells grown in classic 2D culture.

Chapter 2: Materials and Methods

2.1 Nanodiamond Bio-conjugation

A two-step protocol described in (Cordina, Sayyadi et al. 2018) was used with minimal modifications to bio-conjugate lectin proteins to the surface of 120 nm carboxylated HPHT nanodiamonds which were a generous gift from Dr Philipp Reineck (RMIT University). HPHT nanodiamonds have a broad size distribution (30-150 nm) and are monocrystalline, therefore strong acid washes and air oxidation can readily purify them (Mochalin, Shenderova et al. 2011, Lin, Lin et al. 2015). Hence, for carboxylation, 120 nm nanodiamond powder (Nabond Technologies, China) was irradiated by Takeshi Ohshima from Takasaki Advanced Radiation Research Institute (National Institutes for Quantum and Radiological Science and Technology, Japan) with an electron beam of 2 MeV, and to a total fluence of $1 \times 10^{18} \text{ cm}^{-1}$, then it was annealed in vacuum for 2 hours at 800°C and oxidized for 4.5 hours in air at 520°C . For de-aggregation, the carboxylated nanodiamond powder was dispersed in DI water at 1 mg/ml and sonicated using a horn sonicator with a 66% duty cycle for 1 hour at 125 W. *Aleuria Aurantia* Lectin (AAL) was purchased from Vector Laboratories (L-1390), while wheat germ agglutinin (WGA) (L4895) and Tomato Lectin (LEL) were bought from Sigma-Aldrich (Merck) (LO401). FNDs were first pegylated with a PEG₂₂ spacer arm and then the resulting FND-PEG products were conjugated with the desired lectins in the second step as shown in Figure 9.



EDC/NHS chemistry was used twice for the binding of nanodiamonds and lectins (Figure 8). 1-Ethyl-3-(3-dimethylaminopropyl) carbodiimide (EDC) and N-Hydroxysuccinimide (NHS) were used to activate the carboxyl groups on the surface of the nanodiamonds (activated esters). The activated esters then react with amine groups (on the CA(PEG) linker) and an amide bond is formed between the nanodiamond and the CA(PEG). EDC/NHS are used again to activate the carboxyl groups on the PEG linker (forming activated esters). These activated esters react with amine groups on the lectin and an amide bond is formed between the PEG linker and the lectin.

2.1.1 Raw and Bio-conjugated Fluorescent Nanodiamond Characterisation

Protein concentration was measured using 2 µl of the product on a NanoDrop ND-2000 ultraviolet-visible (UV-Vis) Spectrophotometer instrument (Thermo Scientific) with 400 nm wavelength UV-Vis excitation. The measured concentrations were used to calculate an amount of bovine serum albumin (BSA; using $C_1V_1 = C_2V_2$ formula) to be added to the lectin-conjugated nanodiamonds in order to help prevent aggregation of the nanodiamond/lectin complexes. Following this, 4 µl of each product was diluted in 1 ml of water and their size distribution and zeta potential were measured by dynamic light scattering (DLS) using Zetasizer Nano ZS with a 633 nm laser source (Malvern Instruments). FITC-labelled lectins of each type were additionally bio-conjugated to FNDs, and bath-sonicated for 10 minutes in order to assess fluorescent co-localisation, as a sign of successful conjugation, and stability after sonication. AAL-FITC (FL-1391) was purchased from Vector Laboratories, while WGA-FITC (L4895) and LEL-FITC (Lo401) were purchased from Sigma-Aldrich/Merck. An Olympus IX83 widefield fluorescent microscope configured at magnification of 40X was utilised to image FNDs conjugated to each of the FITC-lectins with detector filters of FITC (ex 494 nm; em 518 nm) and nitrogen vacancy nanodiamond (ex 532 nm; em 617 nm).

A Philips CM10 brightfield transmission electron microscope (TEM) was additionally used to assess sizing and aggregation of raw and bio-conjugated nanodiamonds. Sonicated versus non-sonicated nanodiamonds were compared by TEM in order to evaluate the effect of sonication on these properties. Sonicated and non-sonicated raw and bio-conjugated nanodiamonds were washed 5 times with Milli-Q water and then suspended in distilled H₂O. The samples were then dried and dropped on pioloform-coated 300 mesh copper grid for imaging at the magnifications of 5800~92000 with an accelerating voltage of 100 kilovolts.

2.2 Cell Culture

In this project, 3 cell lines were utilised for testing representing different types of brain cells: rat PC12 neurons, human U87-MG astrocytes and mouse BV-2 microglia phenotype cells. PC12 cells were obtained from ATCC (CRL-1721), U87-MG from ATCC (HTB-14), and BV2 cells were a generous gift from Professor Gilles Guillemin (Macquarie University, Sydney, Australia). These cell lines were each grown in complete Dulbecco's Modified Eagle's Medium (DMEM) with high glucose, 10% Foetal Bovine Serum (FBS) (10437028 Gibco life technologies, USDA-approved regions), and 1% antibiotic-antimycotic (AA) (10,000 IU/ml penicillin, 10,000 µg/ml streptomycin and 25 µg/mL of Fungizone® Antimycotic; 15240062 Life Technologies) with the addition of 5% Normal Horse Serum (H1138 Sigma; Australian Origin) for PC12 cells. Cells were maintained in a humidified incubator with 95% air and a 5% CO₂ gas at 37° C.

2.2.1 2D Cell Culture

Cells were cultured aseptically in Greiner Bio-One Cellstar T75 tissue culture flasks, sterile with plug seal caps (Mfg Part Number: 658170) in biosafety cabinets. All cells were sub-cultured for further experiments onto sterile, RNase-free coverslips (22mm x 22mm) for 24-48 hours in 6 well plates.

2.2.2 3D Cell Culture

For culturing cells in 3D, an acellular three-dimensional structure was made by decellularisation of sheep brain tissues obtained from a local abattoir, provided and sliced into pieces using surgical blades (Figure 10).



Figure 10. Sliced sheep brain tissue. A sheep brain hemisphere sliced into 4 pieces to be decellularized and used as 3D scaffolds for cell culture.

Each sliced brain scaffold was separately placed into a Falcon™ 50mL conical centrifuge tube, labelled with a number and date. A solution of sodium dodecyl-sulphate (SDS) 0.1% in milli-Q water plus 1% AA was made for washing the tissues. Each tube that contained a slice

of brain was filled with the solution to 35ml and incubated on a shaker at a speed of 90 rpm for 3 hours (Figure 11). After 3 hours, the solution in each tube was freshly replaced and tubes were incubated overnight on the shaker.



Figure 11. Decellularisation of brain tissues on the shaker. The brain tissues and SDS/PBS media were placed in falcon tubes and placed with an orientation of 90° with the shaker in a box on top of it, and the speed was set on 90 rpm for them to shake between daily washes and overnight.

The SDS washing solution was changed twice daily for 1 week to complete decellularisation, until solution and tissues were clear (Figure 12). The solution in each tube was then changed in aseptic biosafety cabinet conditions in a physical containment level 2 laboratory with autoclaved forceps into autoclaved 1X PBS+ 1% AA and placed into new sterile falcon tubes to remove all SDS. After a few times changing the 1X PBS+1%AA, when there was no more foam or cloudiness observed in the tubes, the tubes and 1XPBS+1%AA solution were changed, and the Falcon tubes were transferred into a fridge until use. All scaffolds were incubated for 2 hours in a solution of 0.04% peracetic acid (PAA) and 4% ethanol in filter sterilized Milli-Q aseptically in a biosafety cabinet. Scaffolds were washed 3 times with autoclaved 1XPBS +10%AA and placed into a new petri dish following each wash before subsequently being cut into 2mm x 2mm x 2mm pieces. The scaffold sections were placed one per well into 24 well-plates and sterilised with ultraviolet light for 45 minutes, rotated manually with autoclaved forceps and sterilised again with ultraviolet light for a further 65 minutes prior to use. Following this, 1ml of complete DMEM with high glucose, 10% Serum FBS and 1% AA with the addition of 5% Normal Horse Serum for PC12 cells was added into each well plate containing a scaffold, and they were incubated at 37° C and 5% CO₂ until use. All plates were monitored for contamination of fungi or surviving cells by observing that the colour of media did not change to orange, brown or yellow from red or pink.



Figure 12. Decellularization of sheep brain tissue over time. Tissues were washed twice daily and shaken with 90 rpm between washes. In addition to tissue changes over time, the changes to the colour of media was observed, that was due to the cells being washed out of the tissue into the media until all cells were washed out on day 8.

Each cell line was first grown in 2D in sterile Greiner Bio-One Cellstar T175 tissue culture flasks with plug seal caps using the conditions described above to yield a high number of cells. Upon confluency, the number of viable cells were counted using flow cytometry with a Muse® Cell Analyzer (Millipore Merck) count and viability assay kit (Millipore 2012). The media of empty sterilised scaffolds was removed from each well, leaving the scaffolds semi-dry for 20 minutes to better absorb cells. Scaffolds were seeded with approximately 100,000 cells in 30µl of media (Shojaie, Ermini et al. 2015) per scaffold for optimal density following 14 days of growth (Burns, Lü et al. 2014) without the addition of any growth factor supplementation. The scaffolds were stored in a humidified incubator with 37°C and 5% CO₂ for 14 days, and their media was changed every 2 days.

2.3 Labelling and Staining of Cells

2.3.1 2D Samples

A master mix was prepared containing 10µl of lectin-conjugated nanodiamonds per 1 ml of 1X Dulbecco's Phosphate Buffered Saline (PBS, Modified, without calcium chloride and magnesium chloride, liquid, sterile-filtered, suitable for cell culture; Sigma; D1408; 10X made to 1X by dissolving 5ml in 45ml Milli-Q water). Alternatively, a master mix of FITC-conjugated lectins was made using 2µl of lectin-FITC per ml of 1X PBS. Cells were sub-cultured onto glass coverslips for 24-48 hours and stained in parallel for each lectin-nanodiamond conjugate or their corresponding lectin-FITC (one condition per well). Labelled cells were incubated at 37°C and 5% CO₂ for 24 hours. After 24 hours of incubation, media was removed, cells were washed with 1X PBS prior to 10 minutes fixation on a shaker with 4% formaldehyde solution (F8775, Sigma, diluted in Milli-Q water). Coverslips were washed 3 times with 1X PBS and mounted onto slides with 26 x 76mm area and 0.8-1.0mm thickness using ProLong™ Glass Antifade Mountant with NucBlue™ stain (P36981). These experiments were repeated 3 times and the resulting staining was observed and imaged first using a widefield Olympus IX83 inverted fluorescent microscope at 40X magnifications then on an Olympus FV1000 Confocal Scanning Microscope at 100X magnification. The IX83 microscope is a modular system with inverted objectives and a 100W halogen lamp and was equipped with a DP80 camera with a 1.4-megapixel monochrome charge-coupled device (CCD). The 40X and 60X objectives (with Olympus immersion oil: part# Z-81012) were used in this study with the following filter specifications: DAPI (ex 364 nm; em 455 nm), FITC (ex 494 nm; em 518 nm) and nitrogen vacancy nanodiamond (ex 532 nm; em 617 nm). The Olympus Fluoview FV1000 IX81 Inverted Scanning Confocal Microscope equipped with four laser diodes (405, 473, 559 and 635) was used for final imaging of 2D samples to be analysed with IMARIS software. Fluorescent excitation, high voltage (HV), gain and offset setting for each channel are shown in Table 1. Cells were viewed and imaged using a 100x

Channel	Excitation (laser power)	HV (V)	Gain (X)	Offset (%)
DAPI	405 nm (4.0%)	465	1.0	12
FITC	473 nm (2.0%)	607	1.0	12
Diamond	559 nm (4.0%)	693	1.0	12

Table 1. Confocal microscope parameters. Settings were unchanged during the imaging of different slides.

objective, with a scanning speed of 8.0 $\mu\text{s}/\text{pixel}$, to assess attraction of FITC labelled and FND labelled lectins in 2D.

2.3.2 3D Samples

Labelling of the 3D scaffolds was conducted similarly to 2D samples, using the master mix concentrations and conditions described above. Scaffolds were however not mounted onto slides, and instead 2 drops of NucBlue™ Live ReadyProbes™ Reagent (R37605) was used in each well/ per scaffold to stain cellular nuclei. In addition, phalloidin-labelled dyes were utilised to stain f-actin filaments in the cells in order to clearly distinguish the cellular areas from potential scaffold autofluorescence. All 3D constructs that contained nanodiamonds were labelled with ActinGreen™ 488 ReadyProbes™ Reagent (R37110). In contrast, constructs containing lectin-FITC, were stained with Alexa Fluor™ 594 Phalloidin (A12381). These scaffolds were imaged on the Olympus Fluoview FV1000 IX81 Inverted confocal scanning microscope used for 2D samples. Fluorescent excitation, high voltage (HV), gain and offset setting for each channel are shown in Table 2. Cells were viewed and imaged using a 60X long working distance objective (UPLSAPO60XS2; W.D.: 0.3 mm) with Olympus silicone immersion oil (Part # Z-81114), and a scanning speed of 4.0 $\mu\text{s}/\text{pixel}$.

Channel	Excitation (laser power)	HV (V)	Gain (X)	Offset (%)
DAPI	405 nm (2.0%)	593	1.0	13
FITC	473 nm (4.5%)	588	1.0	14
Diamond	559 nm (5.0%)	670	1.0	14

Table 2. Confocal microscope parameters. Settings were unchanged during the imaging of different slides.

2.4 Data Analysis

The Fiji (ImageJ) application was used for adjusting the brightness and colour of z-stack confocal microscopic images. Scale were automatically set by the original microscopy image file saved as x-y values, and a scale bar of 50 μm was inserted in the images. The channels were first split, colours and brightness were adjusted, then merged, and stacks were defined by z projection. The maximum number of z slices was 20, however, in some images, a lower number of stacks was used for a clearer illustration of cells in the scaffolds, depending on stacking of the cells.

Imaris image analysis software was used for measurement of fluorescent intensity of nanodiamonds or FITC-labelled lectins by manual thresholding of randomly selected cells (n=3-4 cells per image). The software then measured an average fluorescent intensity per cell of the desired channel in each image (Figure 13). Data from all 2D and 3D samples was collected in Microsoft Excel and analysed for significance with GraphPad Prism 7. A one-way ANOVA test was applied to compare data and draw graphs. The SD of analysed samples was represented as error bars. Statistically significant differences ($P \leq 0.05$) were represented by checking the multiple analysis data: * for $P \leq 0.05$, ** for $P \leq 0.01$, *** for $P \leq 0.001$, **** for $P \leq 0.0001$ and not significant for $P \geq 0.05$.

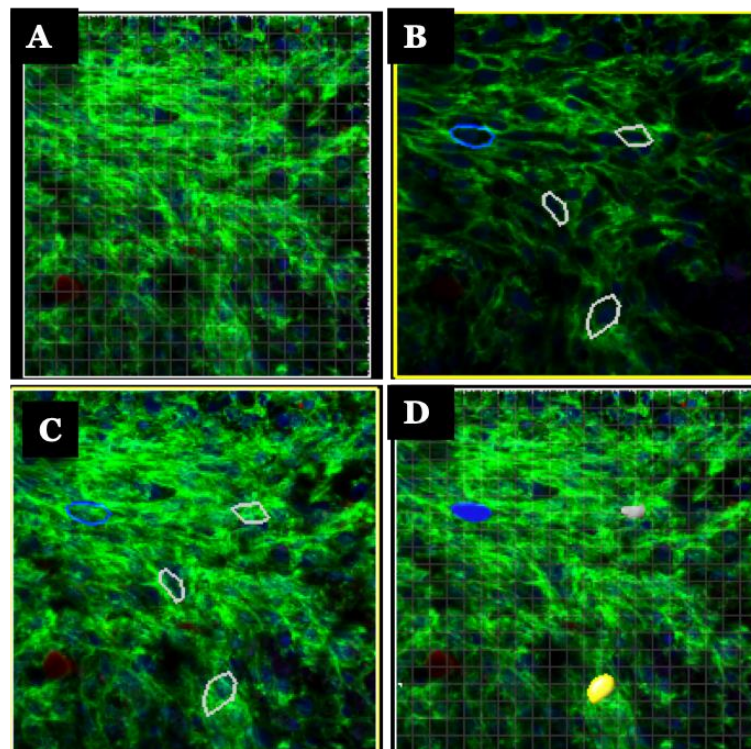


Figure 13. Imaris image analysis software surface creation. Surfaces were created for measuring cell fluorescent intensity in each image. **A.** Sample z-stacked image of a 3D construct with U87-AAL-FND. **B.** Random cells were manually selected by thresholding using the brush tool from a slice of z-stack where the cell boundaries were clearly visible. **C.** The drawn lines were copied to all of the slices of the image. **D.** Surfaces were created.

Chapter 3: Results

3.1 Characterisation of Bio-conjugated Nanodiamonds

After conjugation of 120 nm nanodiamond samples with each lectin (AAL or WGA or LEL) using EDC/NHS chemistry and PEG spacer arm, conjugated nanodiamonds were measured by reading the linear UV-Vis absorbance at 400 nm using the NanoDrop instrument in order to calculate the amount of BSA in PBS (1mg/ml and 5mg/ml) to be added for dilution (Table 3). The size of the final lectin bio-conjugated and raw nanodiamonds particles was measured by dynamic light scattering (DLS) and TEM microscopy to assess particle aggregation before and after sonication. FITC labelled lectins of each type were furthermore conjugated to a subset of nanodiamonds and imaged by microscopy in order to assess the successful conjugation of lectin to particles.

3.1.1 UV-Vis Absorbance and DLS

UV-Vis readings of nanodiamonds in duplicate indicated that the desired concentration (0.311 mg/ml), which was previously calculated by Beer Lambert law of absorbance, was achieved. The amount of 1x and 5x BSA in PBS required to be added was calculated. Then, a second UV-Vis reading was done to test the concentration change and to calculate the amount of BSA to be added for a closer concentration to 0.311 mg/ml (Table3).

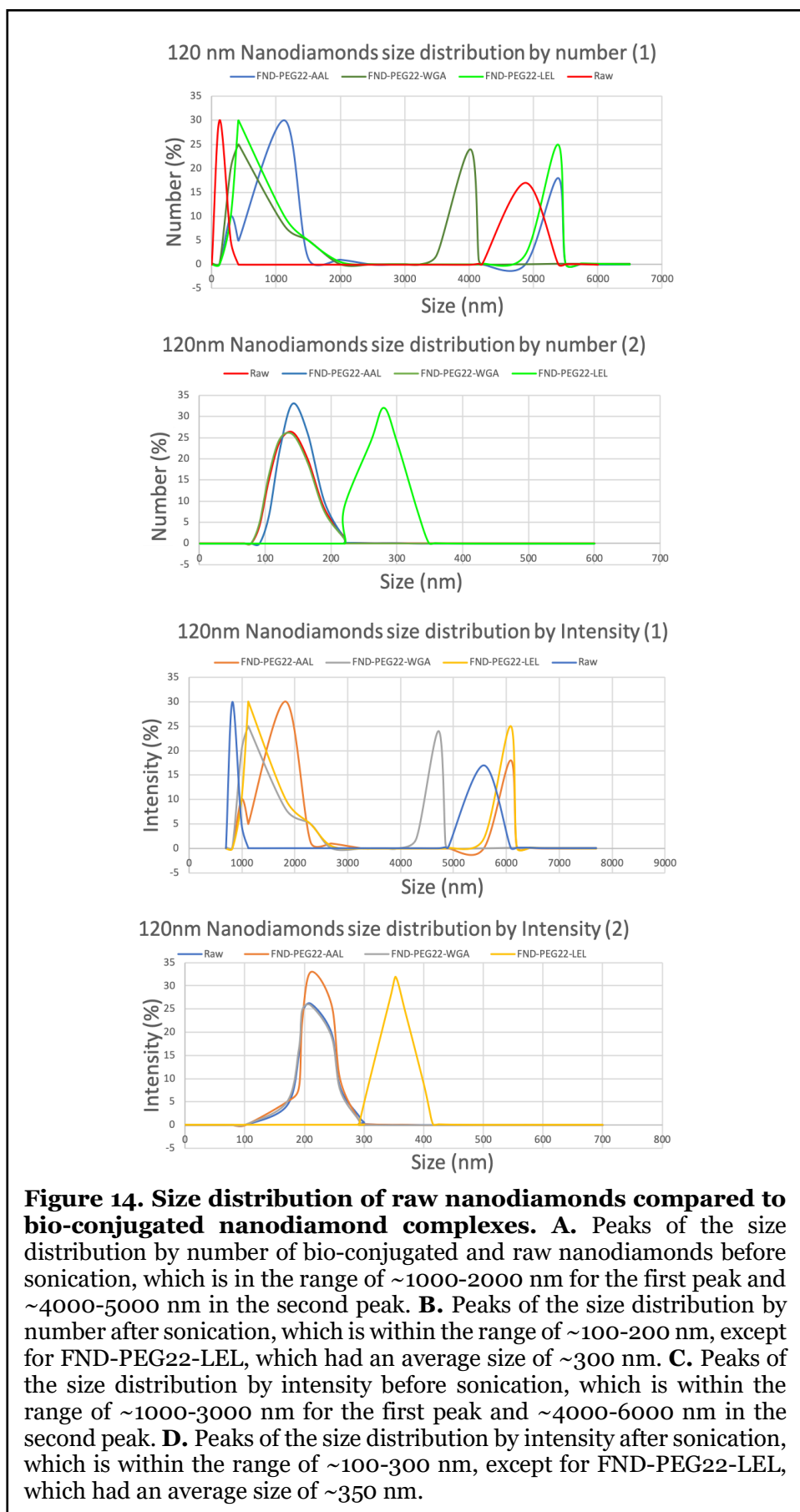
Sample	C1	V1	C2	V2	Add 1xBSA
120nm FND-PEG-AAL	0.711	150.48	0.311	344.02	193.54
120nm FND-PEG-WGA	0.7025	131.10	0.311	296.15	165.04
120nm FND-PEG-LEL	0.3355	115.99	0.311	125.13	9.13

Table 3. Second time calculation for adding BSA containing phosphate buffer saline.

C1 is the reading from NanoDrop instrument, UV-Vis at 400nm. V1 equal to previous calculation final volume. C2 is constant as before. V2 is the second final volume calculated from ($C1 \times V1 = C2 \times V2$). The amount of 1xBSA to be added is calculated from the subtraction ($V2 - V1$).

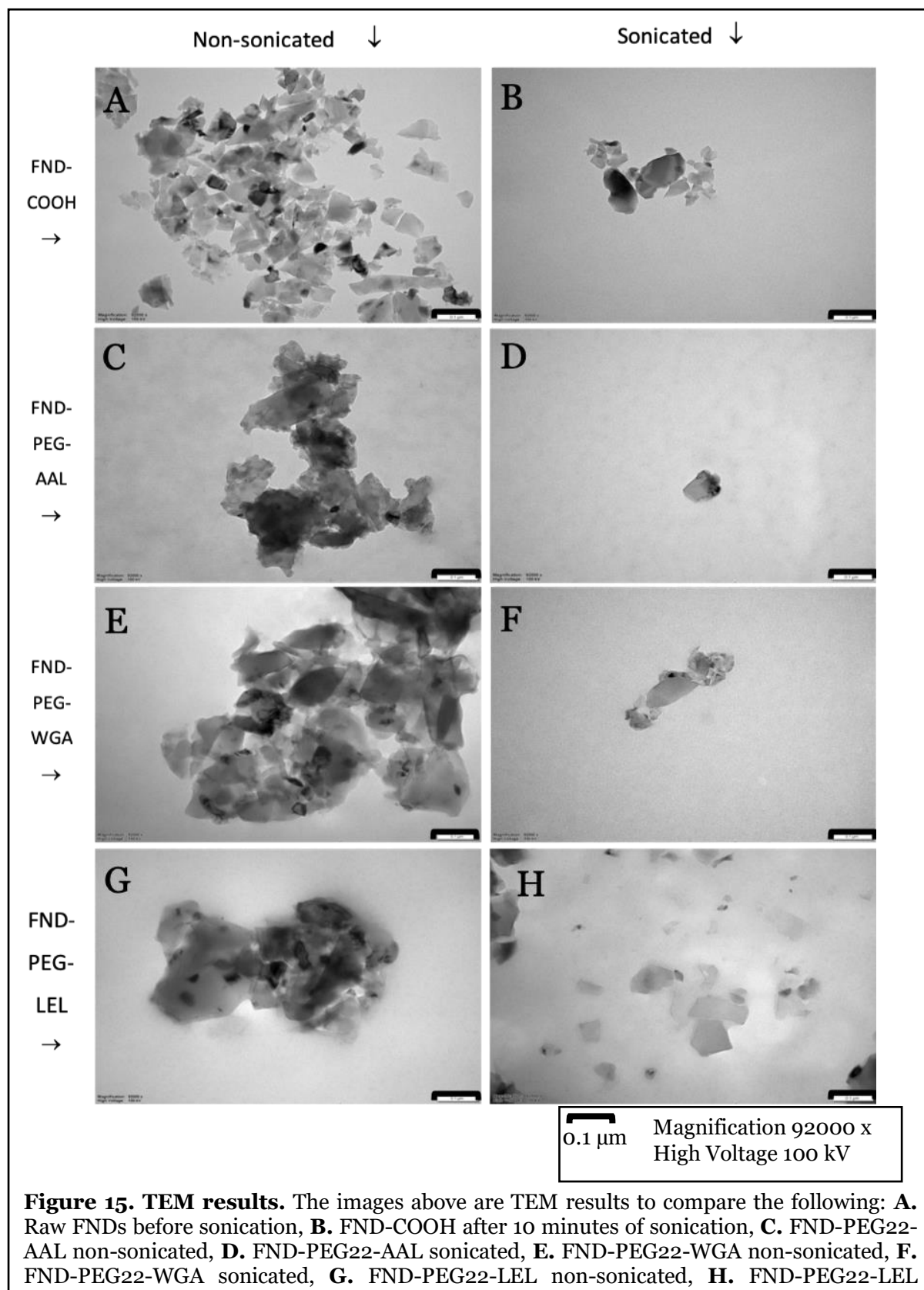
Size distribution by number and intensity of raw nanodiamonds (Raw FND) and conjugated nanodiamonds (FND-PEG22_lectin) was measured by DLS using a Zetasizer instrument after sonication (Figure 14). The sizes of most nanodiamond complexes were ~150 nm with

an intensity of ~ 200 nm after bath-sonication for 10 minutes, indicating that they were not aggregated with the exception of the LEL-FND complex.



3.1.2 Transmission Electron Microscopy

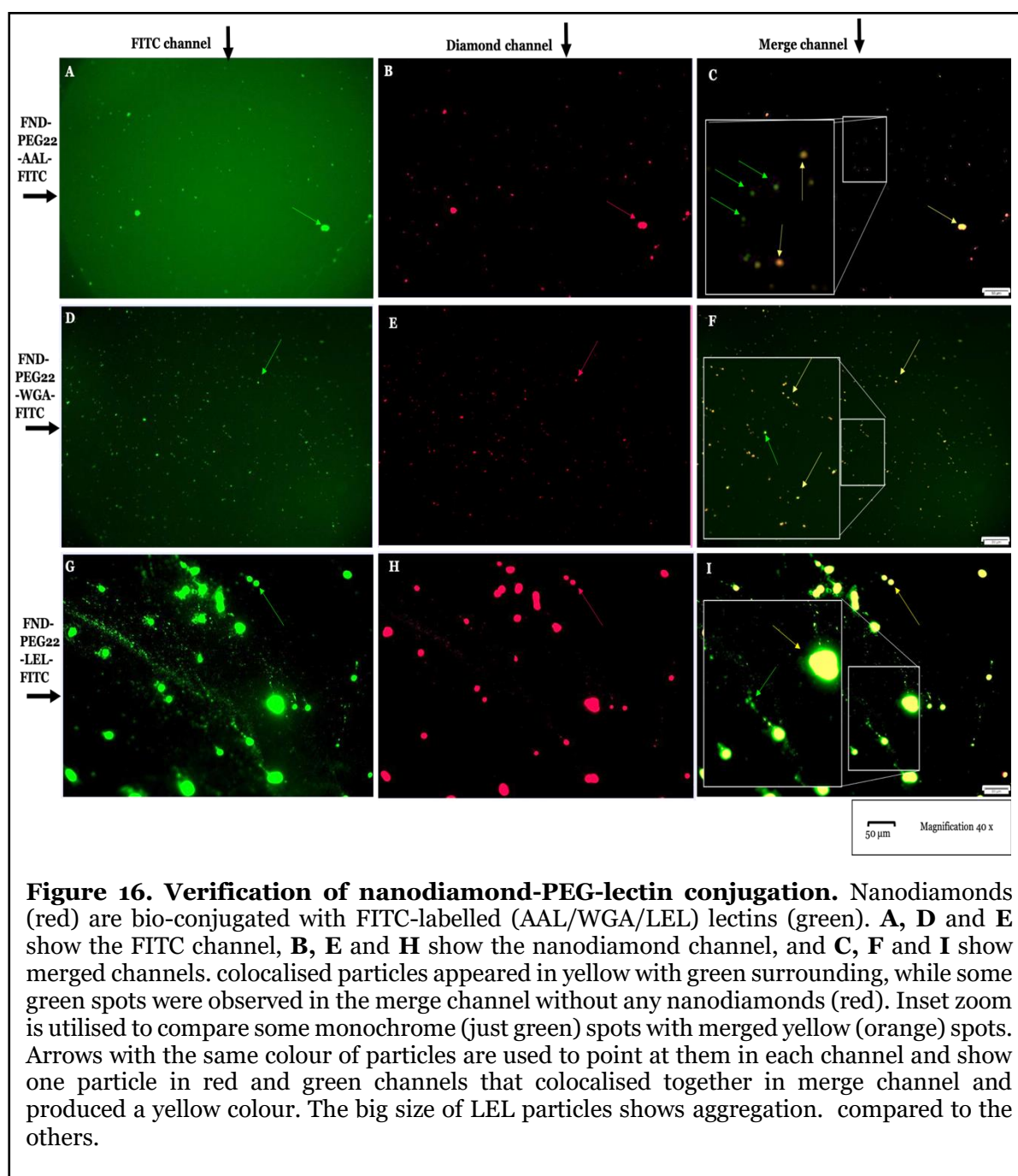
Raw (carboxylated) and bio-conjugated nanodiamonds were imaged on TEM sample grids before and after bath sonication, to compare their size and aggregation.



All nanodiamonds were aggregated before sonication (Figure 15), which was substantially reduced following a 10-minute bath sonication. Raw nanodiamonds presented in clear geometric shapes, even in their aggregated form, while bio-conjugated nanodiamonds are surrounded by lectin proteins, clouding their shapes. However, sonicated nanodiamonds that were bio-conjugated were more similar in appearance to raw nanodiamonds, indicating the possibility that a breakage of their bonds may have occurred with lectins following sonication.

3.1.3 Verification of Nanodiamond Bio-conjugation

To test the possibility of a loss of lectin from the nanodiamond surface following -



sonication, widefield microscopy was used to assess co-localisation of nanodiamonds with FITC-lectins after 10 minutes of bath-sonication (Figure 16). Although there is a possibility of nanodiamonds to emit in the green channel due to the number of their nitrogen vacancy centres, by looking closely at the yellow spots it can be observed that the centre is yellow, and the surrounding is green, meaning that the size and locality of the red and green emissions are different, which is also observed in red and green channels. Our findings indicated that almost all of the nanodiamonds were successfully bio-conjugated with FITC labelled lectins and this conjugation remained almost stable after bath-sonication. Consistent with the DLS/Zetasizer and TEM findings, LEL FND conjugates were the most aggregated complexes. Only a small number of lectins were not conjugated to nanodiamonds as seen in the merge channels.

3.2 CNS Cell Specific Targeting with Lectins

Lectin-conjugated (AAL/WGA/LEL) nanodiamonds (FND) and raw nanodiamonds (non-conjugated nanodiamonds) were incubated for 24-48 hours with live brain cells in 2D and 3D experimental conditions as described in Chapter 2 and were compared in parallel to the commonly used fluorescent (FITC) conjugated lectins. All cells were imaged by confocal scanning microscopy at 100X for 2D samples and 60X for 3D grown cells. The resulting microscopy images were qualitatively and quantitatively assessed by confocal microscopy and Imaris software for their fluorescent intensity and analysed in GraphPad Prism software.

3.2.1 Qualitative Results

To compare the attachment of each lectin to each cell line, coverslips of U87-MG, PC12 and BV2 cell-lines, representing malignant astrocytes, neurons and microglia respectively, were treated by each of the following separately: AAL-PEG22-FND; AAL-FITC; WGA-PEG22-FND; WGA-FITC; LEL-PEG22-FND; LEL-FITC; raw-FND. The coverslips were incubated with labelled lectins for 24 hours and then fixed and stained with NucBlue for imaging the nuclei of the cells and locating the cells. The control group was each untreated cell-line stained with NucBlue.

Figures 17 and 18 show the comparative result of the labelling of the different cells grown in 2D cultures with each lectin. For raw FND (without lectin) qualitative results compared to lectin-conjugated nanodiamonds binding to each cell line in 2D cell culture please see the supplementary materials. Control samples (without labelling) indicated that the microscopy settings utilised to visualise FND or FITC also captured a significant amount of unwanted

cellular autofluorescence in each channel. The competition of FITC with cellular

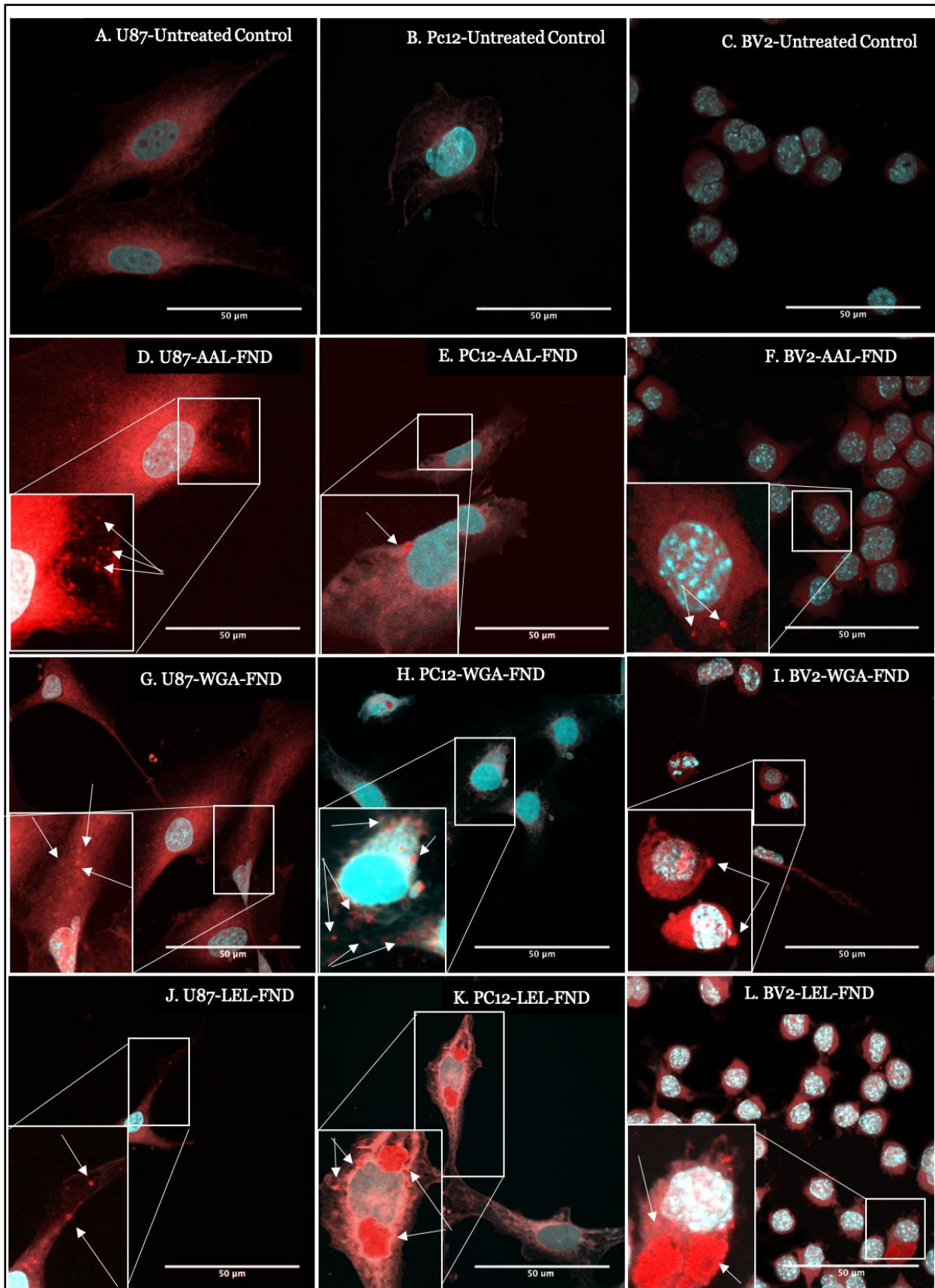


Figure 17. 2D microscopy with brain cell samples with lectin-FND conjugations. A, B and C. Not treated with any lectin as negative controls. To show the nanodiamonds in a bigger scale, some areas are enlarged by inset zoom in lectin-FND treated cell-line images. The white arrows point at some of detected nanodiamonds. The green channel for these images is blocked to show the nanodiamonds clearly.

autofluorescence made it challenging to recognise whether FITC-lectins were successfully

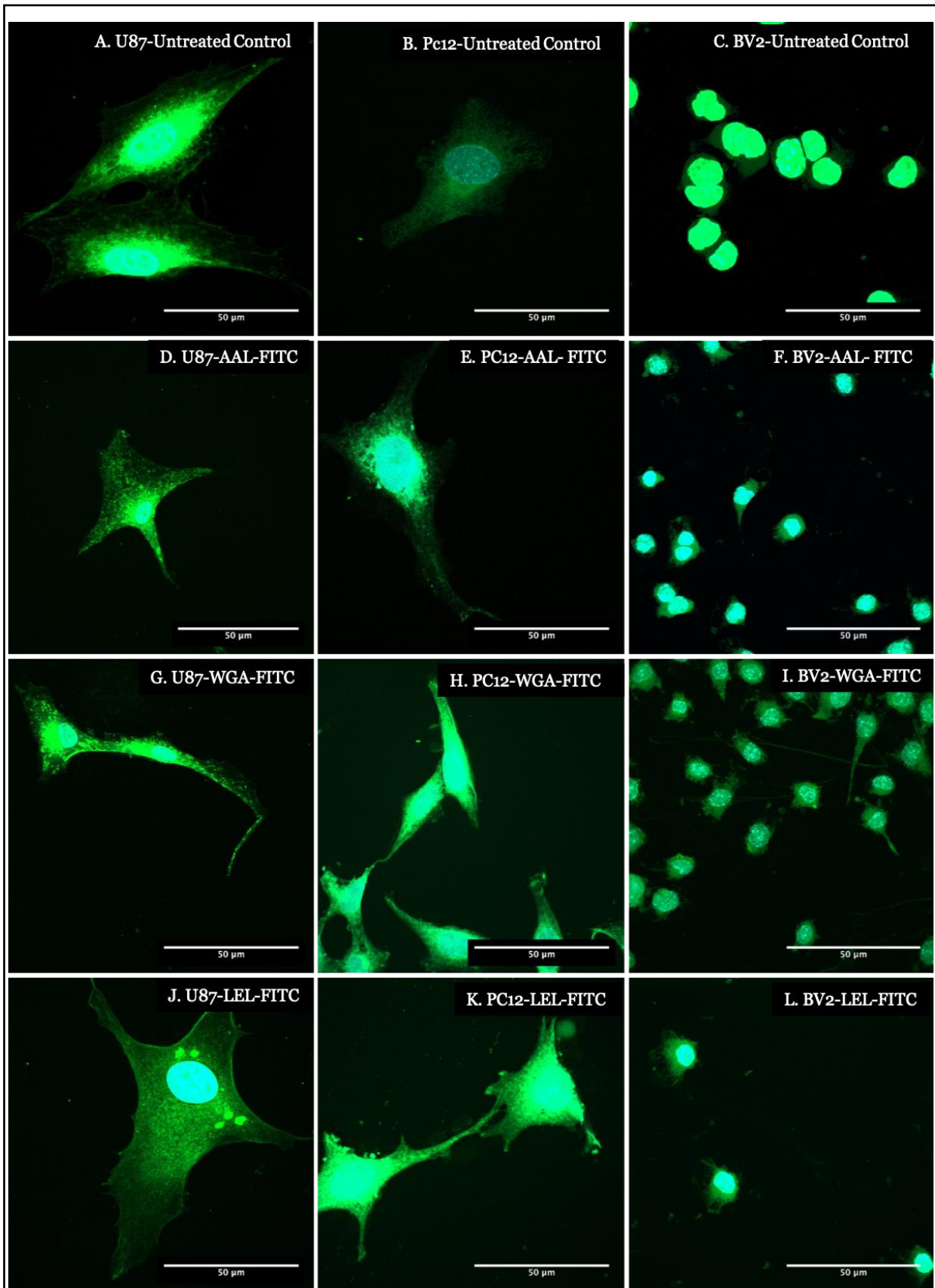


Figure 18. 2D microscopy with brain cell samples with lectin-FITC conjugations. A, B and C. Not treated with any lectin as negative controls. The red channel for these images is blocked to show FITC clearly. However, green autofluorescence of brain cells compete with FITC emission.

attracted by the cells. However, nanodiamonds had brighter emission that could be distinguished as punctate fluorescence within the cell boundaries, making their labelling easier to distinguish than FITC-lectins for the cells grown in 2D cultures. Our findings indicated that AAL is attached more to U87-MG cells compared to the other two cell types, and BV2 has bound more AAL than PC12. This indicates that fucose is expressed more on the surface of glioblastoma multiforme astrocytes in comparison to neurons and microglia, while microglia express more fucose than neurons. Both WGA and LEL are attracted to all of the studied cell-lines similarly, however, LEL conjugated FNDs seem to be more aggregated, and were seen as clumped red particles on the cells, despite being sonicated before the incubation with cells.

The different cell types were grown in the 3D de-cellularised scaffolds for 14 days, and then incubated with lectin-FITC or lectin-PEG-FNDs for 48 hours, fixed, stained and imaged by the same confocal microscope with a 60x long working distance objective. For staining, in addition to NucBlue for the nuclei, Phalloidin was used to stain f-actin filaments to try to differentiate between cells and scaffolds. Where the constructs (scaffolds+cells) were treated with nanodiamonds (emitting in red), Phalloidin-Alexafluor488 was used to show cell boundaries in green, and where cells were treated with FITC (emitting in green), Phalloidin-Alexafluor594 was used to indicate cell boundaries in red. Hence, the emission colour of cell boundaries could be the different from the lectin labels and distinguishable from each other. As negative control, some scaffolds were not seeded with cells, and were either untreated or treated with the same lectin labels as the cell-seeded scaffolds. The untreated cell-free scaffolds showed autofluorescence in all channels, indicating that the scaffolds autofluoresce before any labelling. To make the nanodiamonds visible, the green channel was not completely blocked, and just set to contrast between the scaffold fluorescence and the nanodiamonds. This method was helpful because the diamonds only emitted in the red channel despite the scaffolds that emitted in all channels, so the difference could be highlighted in the merged channel(Figure 19). The same imaging method was also used to make FITC labels clearer compared to the background autofluorescence (Figure 19). It was difficult however to distinguish FITC from the green fluorescence of the scaffolds. Hence, nanodiamonds were identified as better imaging agents compared to dyes like FITC for labelling and imaging in 3D scaffold models.

Figure 19 shows that nanodiamonds bio-conjugated with both WGA and LEL lectins bind to cell-free scaffolds, with the amount of WGA-FND bound seemingly higher than

those of LEL-FND. The result is not surprising because the brain ECM scaffold has been found to contain hyaluronic acid and this glycosaminoglycan is composed of D-glucuronic acid and GlcNAc monomers (Ruoslahti 1996) which would thus bind both WGA and LEL. Brain scaffolds retain high amounts of hyaluronic acid after decellularisation (Zhu, Tang et

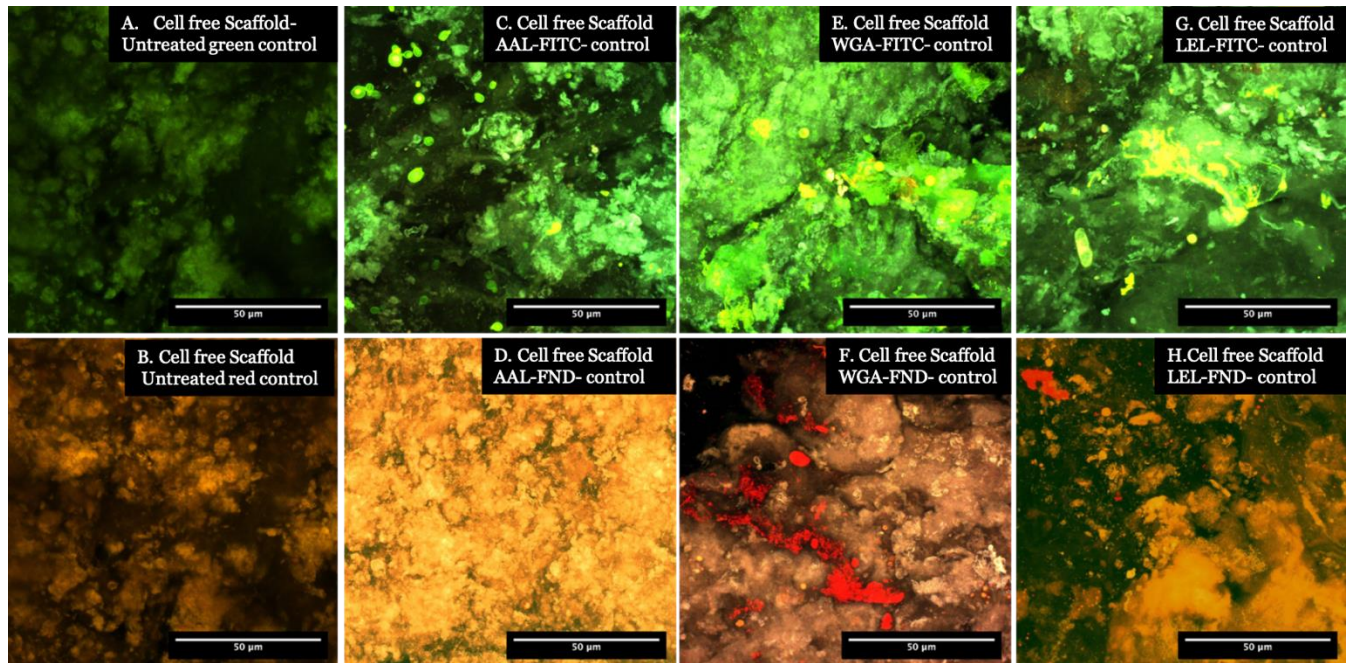


Figure 19. Cell free control 3D scaffolds. The 3D scaffolds in this figure were used as control without seeding any cells in them. **A** and **B**. Untreated control: The green and orange colours are from the autofluorescence of the extracellular matrix. **A**. red channel is deemed to show the green autofluorescence, **B**. Green channel is deemed to show the red autofluorescence. Scaffolds in images **C-H** are treated similar to the experiments (with lectin-FITC and lectin-FND). Scaffolds in the images **C**, **E** and **G** are treated with FITC, therefore the red channel is deemed to show the green fluorescence clearly. The yellow spots can be caused by the localization of the brightest emissions of red and green in the merged channel. In images **D**, **F** and **H** the scaffolds are treated with FNDs which emit red light, therefore the green channel is deemed to show the red fluorescence more clearly. Deeming the other channel instead of blocking it completely, helped to distinguish the nanodiamonds from the scaffold pure red autofluorescence, by the contrast of nanodiamond emission from scaffold emission in the merged channel. Interestingly, images **F** and **H** show that WGA-FND and LEL-FND are absorbed by the empty scaffolds.

al. 2015). Hence, these lectins have targeted those sugars in the structure of the scaffolds as well as the same monosaccharide GlcNAc found on the surface of cells, which makes these lectins not useful for the purpose of targeting sugars on the surface of the cells grown in these 3D scaffolds. Importantly however, the AAL lectin conjugated nanodiamonds do not show any binding to the cell-free scaffolds and thus offer a means of visualising the cells in the 3D scaffold.

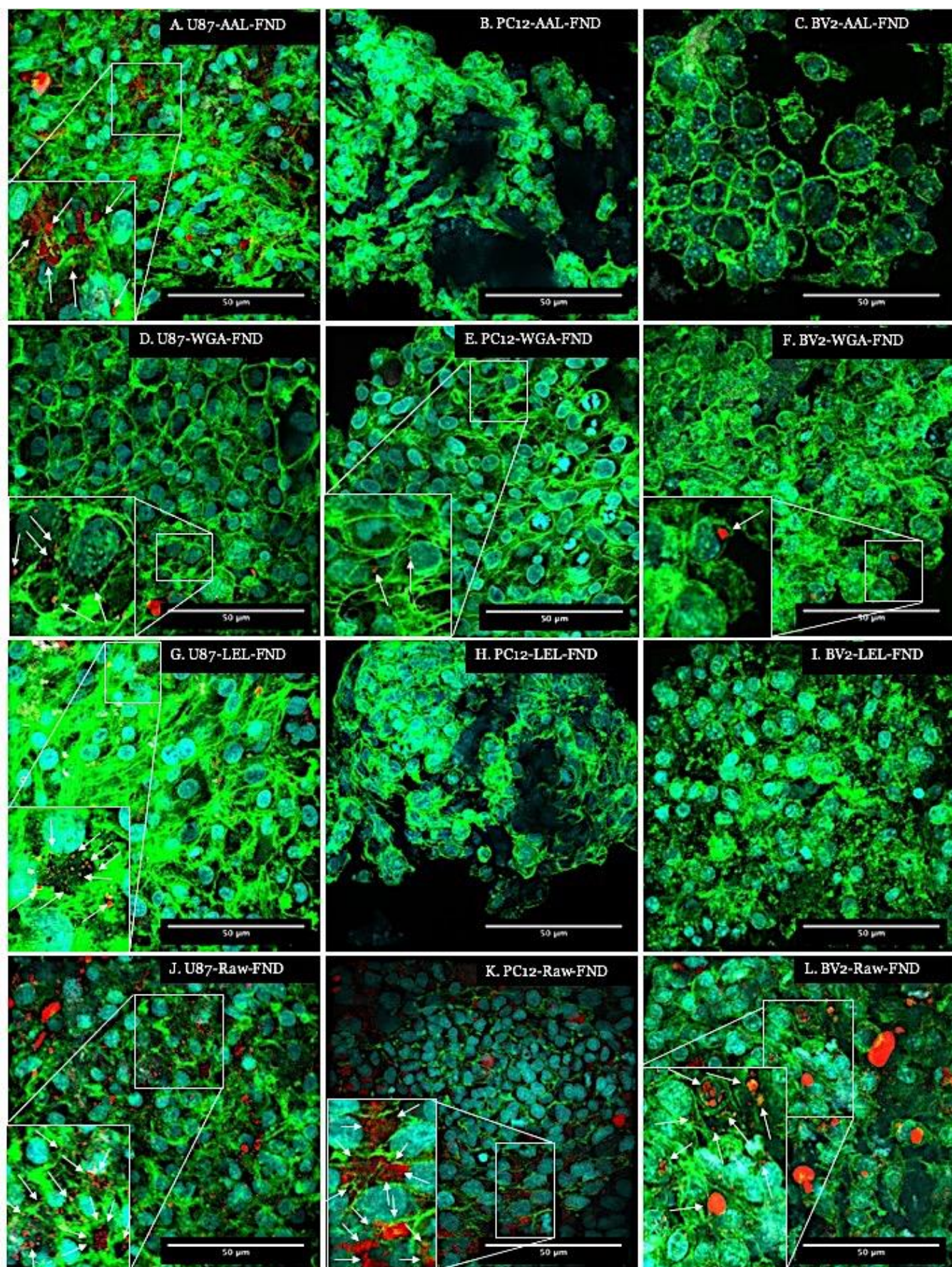


Figure 20. 3D microscopy with brain cell samples with lectin-FND conjugations and raw nanodiamonds. These images are captured from scaffolds with brain cells, that were treated by FND-conjugated lectins as well as non-conjugated nanodiamonds (raw FND). DAPI was used to stain nuclei (cyan), and phalloidin-Alexafluor488 was used to stain f-actin filaments to represent cell boundaries. It was aimed to differentiate between cells and scaffolds by staining cells with phalloidin in green. Inset zoom and white arrows in images with nanodiamonds are used to show nanodiamonds in a bigger scale.

After investigating the results on the control scaffolds, the lectin binding was compared. For reducing the background autofluorescence of the scaffolds, the parts that contained higher number of cells were imaged layer by layer using z-stack feature of the microscope.

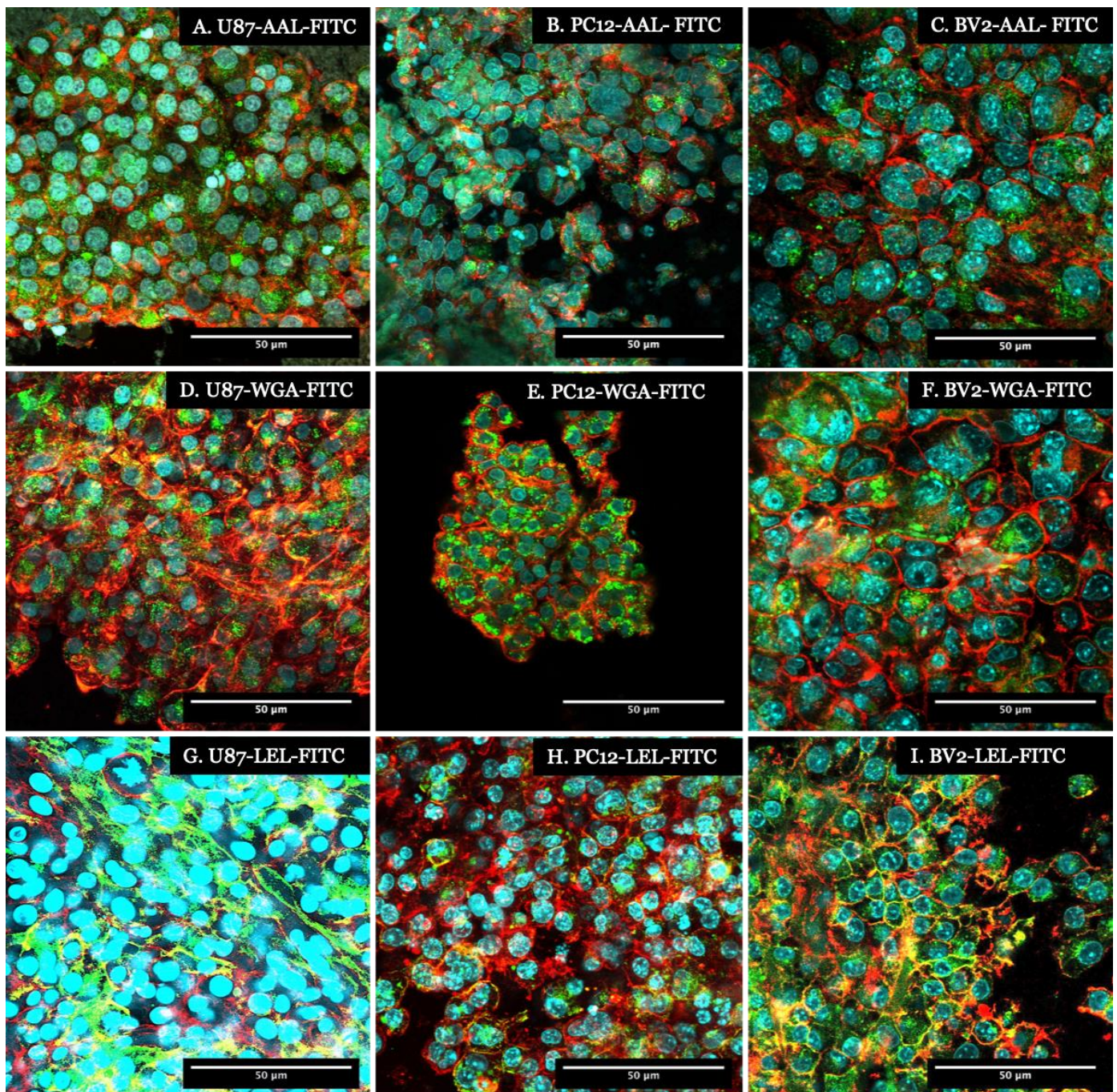


Figure 21. 3D microscopy with brain cell samples and lectin-FITC conjugations. These images are captured from scaffolds with brain cells, that were treated by FITC-conjugated lectins. DAPI was used to stain nuclei (cyan), and phalloidin-Alexafluor594 was used to stain f-actin filaments to represent cell boundaries. It was tried to differentiate between cells and scaffolds by staining cells with phalloidin in red. In U87-LEL-FITC colocalization of phalloidin in red and FITC in green was observed.

Figure 20 shows the constructs that were treated with bio-conjugated nanodiamonds, and stained with Phalloidin-Alexafluor488, so that the nanodiamonds are visible in red and f-

actin filaments define the cell boundaries in green. The cells are piled on top of each other in different layers. Some of the stacks are omitted to indicate the cells and nanodiamonds more clearly. The white arrows in the inset zooming areas point to the detected nanodiamonds.

The highest number of nanodiamonds attached as AAL-PEG22-FND to the U87-MG cells, which may reflect the upregulation of fucose on the surface of glioblastoma astrocytes. All of the three FND-lectins bound to U87-MG 3D grown cells, whereas PC12 and BV2 cells only showed attachment of WGA-PEG22-FND. Although binding of WGA to all of the three cell lines is seen, it is not clear whether the WGA-PEG22-FNDs have bound to the hyaluronic acid GlcNAc sugars of the scaffold or to the other GlcNAc and sialic acid sugars on the cell surfaces. No LEL-PEG 22-FNDs are seen to be bound to the PC12 and BV2 cells grown in 3D despite LEL having been seen to bind to the scaffold control (Figure 19).

However, since it was shown that AAL lectin does not bind to the scaffold (Figure 19), it can be concluded that AAL lectin targets U87-MG selectively compared to the other cell lines grown in 3D cell culture. AAL targets fucose which has not been found in the brain ECM .

Figure 21 shows the same experiment with FITC labels in place of FNDs, and f-actins are coloured in red in an attempt to demonstrate cell boundaries by staining them with Phalloidin-AlexaFluor594. Generally, the lectins labelled with FITC (Figure 21) show more binding compared to the lectins labelled with nanodiamonds (Figure 20). For example, AAL-FITC (images A,B, C) and LEL-FITC (images G,H, I) in Figure 20 show binding to all cell-lines, while AAL -FND(images A, B, C) and LEL -FND (images G, H, I) in Figure 21 do not show any binding to PC12 and BV2 scaffolds. These differences could be due to either, or both of, the interference of the emission of scaffolds in green with FITC, and the inability of nanodiamonds to penetrate through the scaffolds and reach to the cells. However, both Figures 20 and 21 indicate similar results about the binding of AAL preferentially to U87-MG cells grown in the 3D scaffolds. To verify these findings, fluorescent intensities per cell were quantified and compared.

3.2.2 Quantitative Results

The microscopic images (three replicates of each condition) were used to quantify fluorescent intensity of cells by Imaris software, by thresholding single cells (n=3 or 4 in each replicate) and creating surface on all of their z slices and collecting data from the desired channel. The data was used on GraphPad program to produce comparable graphs, as shown in figure 22.

Comparisons of Figure 22 charts match with the findings from the microscopic images, except that the green fluorescence intensities from different cell lines are compared as well as their red fluorescence. In qualitative analysis it was challenging to differentiate green fluorescence in various images. The left charts indicate lectin binding to the three different cell lines in 2D growth, and the right charts show the binding of the same lectins to the different cell lines in 3D. The three left bars in each chart represent green fluorescent intensity per cell, and the three bars on the right represent red fluorescent intensity per cell.

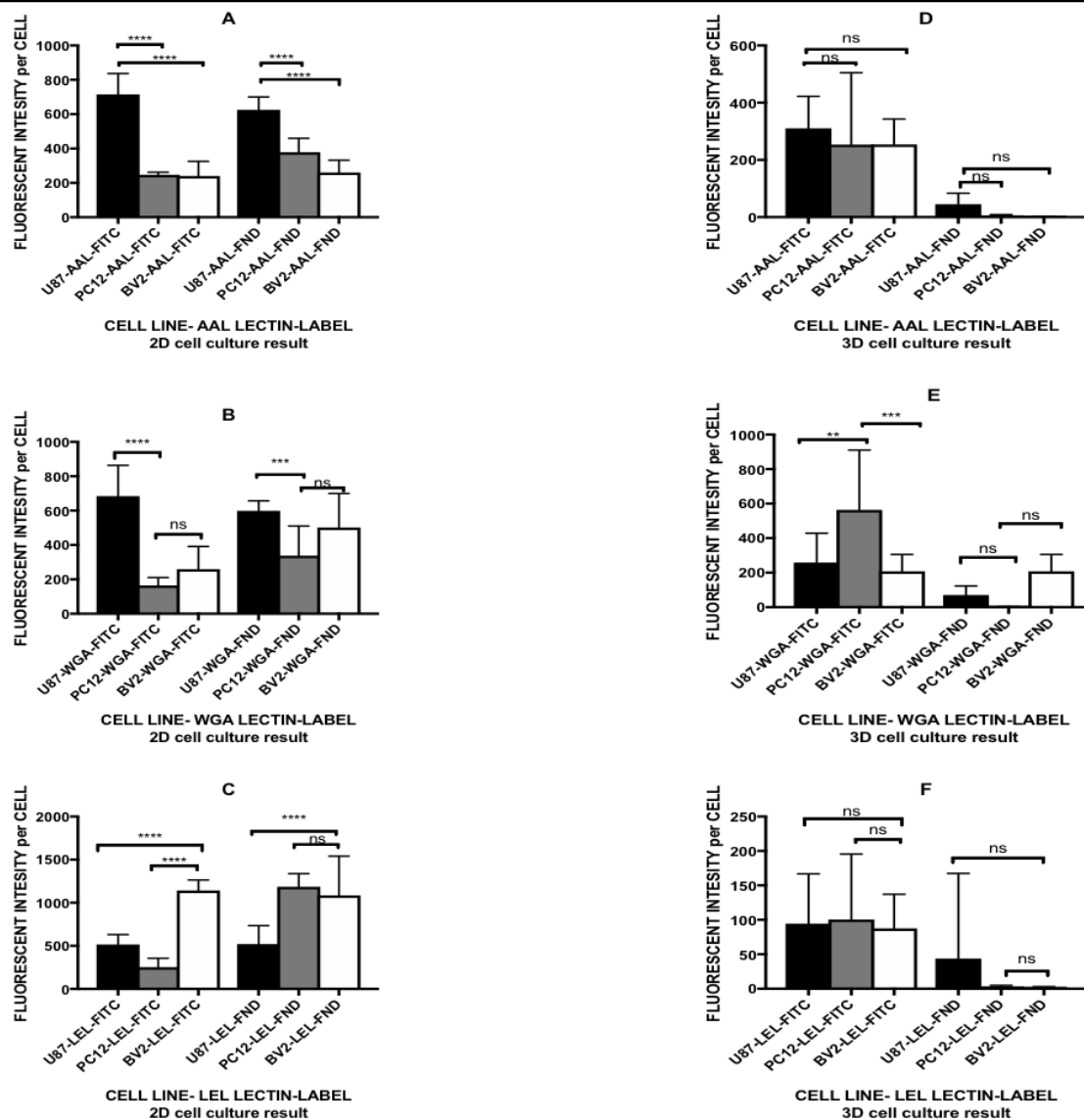


Figure 22. Quantitative results. The attraction of FITC-labelled versus FND-labelled AAL, WGA and LEL lectins by U87-MG, PC12 and BV2 cells in 2D and 3D is shown above. **A, B and C** charts show fluorescent intensity results from 2D cell culture cell lines and **D, E and F** bar charts illustrate the same thing in 3D culture cell lines. The number of cells in this test for **A, B and C** were $n=12$, from 3 images, and 4 cells of each image, and $n=9$ for **D, E and F**, from 3 images and 3 cells on each image. The SD is shown as error bars. Statistically significant differences ($P \leq 0.05$) are represented: * for $P \leq 0.05$, ** for $P \leq 0.01$, *** for $P \leq 0.001$ and **** for $P \leq 0.0001$. The null hypothesis was that AAL will be attracted by u87-MG cells more than the other two cell lines, while WGA was expected to be attracted by all three of them, and LEL to be attracted more by BV2 cells rather than the other two.

The results from 3D grown cells show that nanodiamond binding to the cells was not high, however, U87-MG cells have each lectin attached. Moreover, AAL is attached to U87-MG cells more than to the other two cell lines in both 2D and 3D growth, whether labelled by FITC or FND. The 3D cell binding results of AAL lectin are the most reliable because there is no AAL binding to target fucose in the cell-free scaffolds. In contrast, WGA and LEL binding is unclear in the 3D grown cells as both of these lectins are known to bind to the GlcNAc monomers of hyaluronic acid of the scaffolds as was shown in the control qualitative images, and it is not possible to distinguish between the scaffold and cell binding of these lectins in this study. The quantitation charts however show that the fluorescent intensity of AAL and WGA that were attached to U87-MG 3D grown cells were almost equal and nearly twice more than LEL binding in both FITC and FND labelled lectins in 2D. On the other hand, the fluorescent intensity of LEL that was attracted to BV2 cells was almost 6 times higher than AAL and almost three times higher than WGA comparing the 2D results of both FITC and FND labelled lectins. The fluorescent intensity of lectins attracted to PC12 though, do not show a trackable trend in green and red channels. Nanodiamond-lectin fluorescent intensity per PC12 cell is higher than that of FITC-lectin in 2D.

3.3 Comparison of 2D and 3D

The presence of brain ECM in this experiment has caused some difficulties in the interpretation of the results. For example, the amount of bio-conjugated nanodiamonds with lectins attracted to 3D constructs were significantly lower than that of 2D cultured cells (Figure 23).

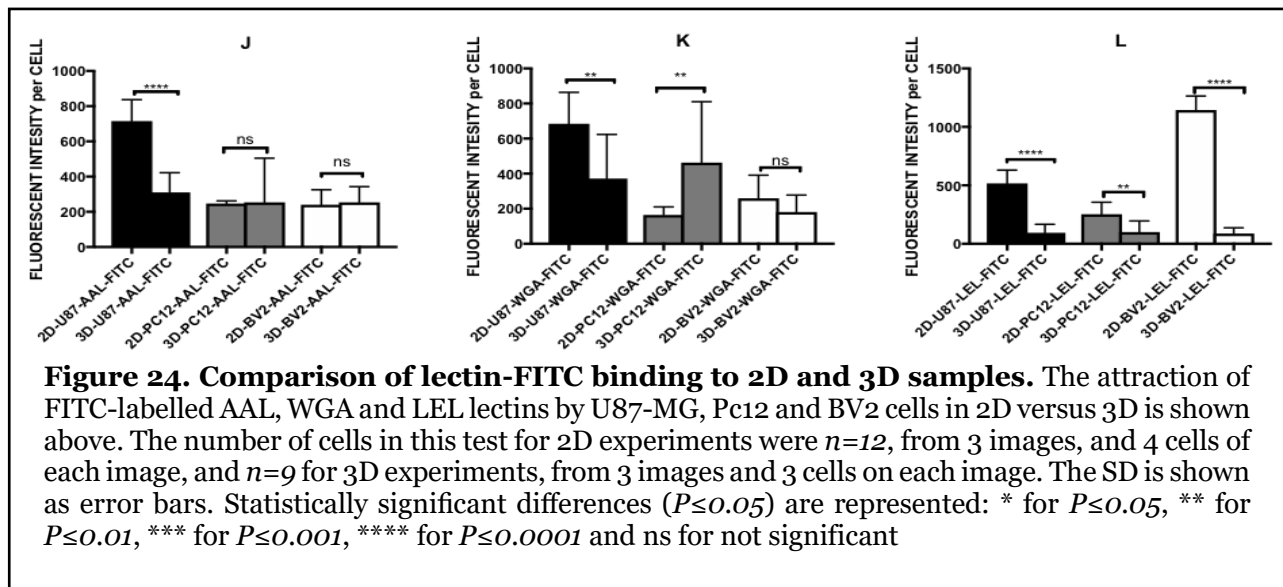
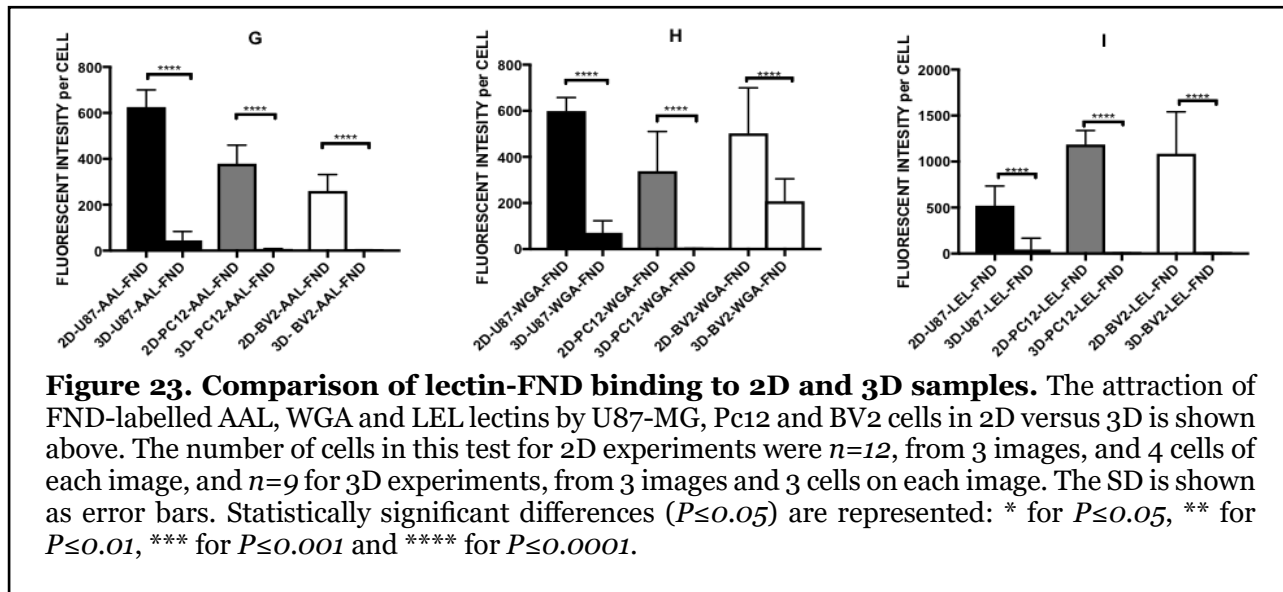


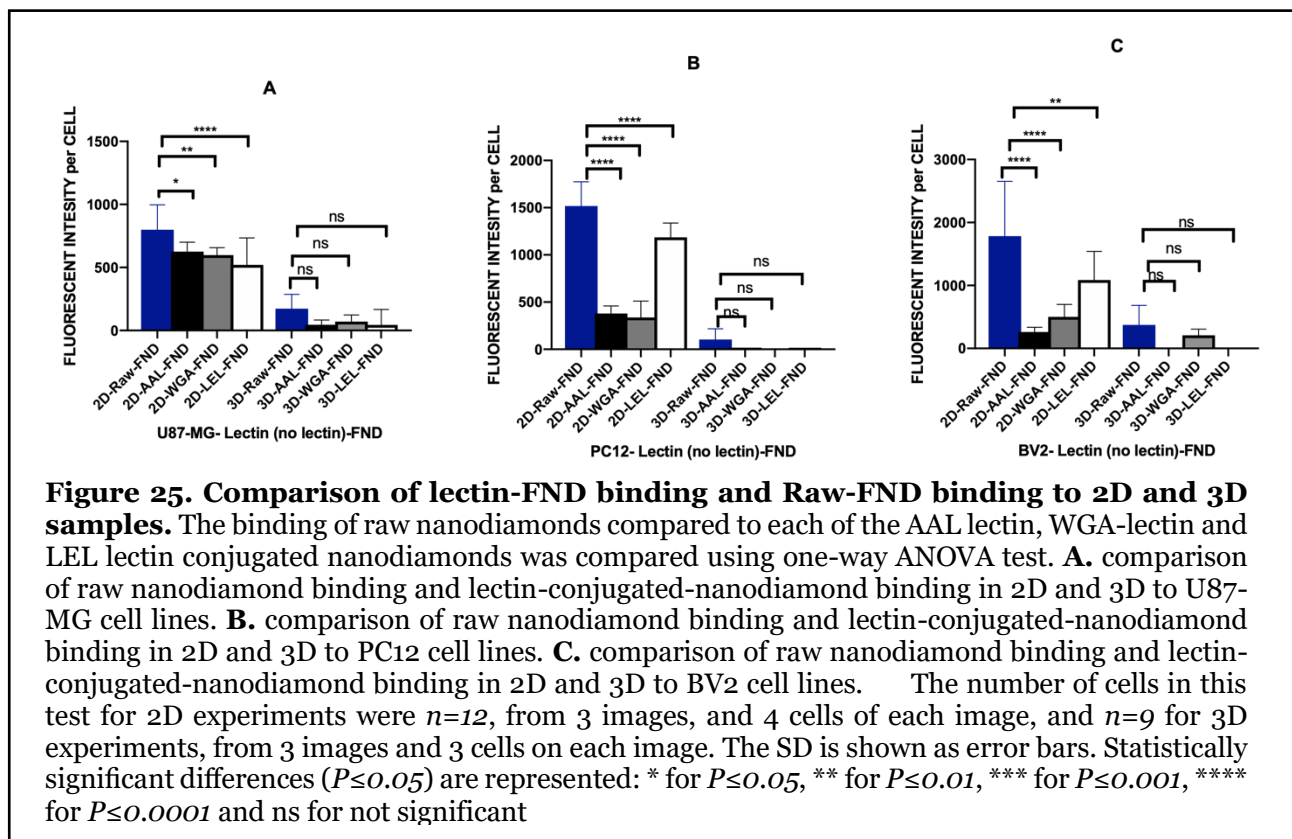
Figure 23 indicates that very low number of lectin-FNDs were attracted to 3D grown cells compared to 2D cell culture. However, this was not the case with labelling with FITC-labelled lectins, as shown in Figure 24. It was shown before that the lectins WGA and LEL

bind to 3D scaffolds and complicate the calculation of fluorescent intensity. Therefore, the only reliable 2D versus 3D comparison would be that of AAL lectin.



The amount of AAL -FITC attached to the cells in 2D and 3D by PC12 and BV2 cells is almost the same, while this amount in U87-MG cells is significantly higher. showing that U87-MG in 2D reacts differently to AAL lectin compared to 3D, by attracting more lectins.

3.4 Comparison of Lectin-conjugated Nanodiamonds and Raw-Nanodiamonds Binding to Cell Lines



The same methods as above were utilized to compare the binding of nanodiamonds to the

cells without being labelled by lectins (raw nanodiamonds) with the binding of all above mentioned lectin conjugated nanodiamonds to each cell line in 2D and 3D (Figure 25). As shown in Figure 25, in both 2D and 3D models a significantly higher level of fluorescent intensity is observed for raw nanodiamonds binding to the cells, rather than the bioconjugated nanodiamonds. The intensity difference shows that the bioconjugation of the nanodiamonds definitely changes the cell-binding results.

Chapter 4: Discussion

4.1 Aggregation of Bio-conjugated Nanodiamonds

Raw nanodiamonds and bio-conjugated nanodiamonds both showed aggregation before being bath-sonicated when analysed by DLS and imaged by TEM, and sonication helped to separate particles from each other. TEM images showed that nanodiamonds had geometric shapes, while bio-conjugated nanodiamonds were clouded by lectins in their aggregated forms, forming clumps. After sonication, all particles were separated into smaller geometric shapes, that caused concern of whether the breakage of the bonds between the nanodiamonds and lectins had occurred during sonication. To verify the conjugation of nanodiamonds with lectins and their stability after bath-sonication, FITC-labelled lectins were conjugated to the nanodiamonds and imaged by a fluorescent widefield microscope to test if the lectins with Fluorescein (green fluorescence) co-localised with nanodiamonds (red fluorescence) as a sign of successful conjugation and stability after bath-sonication. This confirmed that all three lectins were conjugated to the nanodiamonds and that the bond between them was not broken by 10 minutes of sonication. Although some green particles could still be observed in the merge channel without any colocalization with red that could mean the bio-conjugation was not successful or the might have been broken by sonication, the number of colocalised particles was much higher than those monochrome ones, making it very difficult to search for them in the images to point them out. All bio-conjugated nanodiamonds were therefore bath-sonicated for 10 minutes prior to interaction with cells. Some aggregation of the LEL-FNDs was still visible in confocal microscopic images of PC12 and BV2 cells in 2D grown culture. These conjugates were not sonicated for a longer time in this study, as it would affect the consistency of the methods used for the preparation of nanodiamonds with each lectin. However, the aggregation of LEL-FND could have affected the results of fluorescent intensity of cells, as fluorescent intensity increases due to the aggregation of lectin-FITC or lectin-FND (Oshinbolu, Shah et al. 2018). This may explain the higher fluorescent intensity per cell with LEL conjugates.

The stability of the bond between the lectins and nanodiamonds after sonication was verified by widefield microscopy, showing that sonication does not break those bonds between them. Also, the specific binding of lectins to the cells showed that at least some of their function was not disrupted. However, close examination of lectins could not be fitted in this research

to validate if after sonication process lectins went through any damages in their molecular structures or whether a number of them became dysfunctional or not.

4.2 Specificity of Lectins

In this project, three types of lectins were studied for investigation of their cell specific targeting in the brain. *Aleuria Aurantia* lectin (AAL) was used to target fucose to compare the surface of cell types, because fucose is found to be upregulated in glioblastoma astrocytes (Lefranc, Brotchi et al. 2005). Wheat germ agglutinin (WGA) was utilised for targeting sialic acid on the surface of neurons, as sialic acid is expressed in high amounts on the surface of these types of brain cells (Theodosis, Bonhomme et al. 1999). *Lycopersicon Esculentum* lectin (LEL) was chosen for targeting high mannose *N*-glycans on the surface of microglia, because these glycan structures were previously studied as a marker for those cells (Oguri 2005, Villacampa, Almolda et al. 2013). Nevertheless, not all lectins are only specific for one type of sugar residue, which makes it complicated to use them for targeting, imaging and drug delivery purposes unless they have high specificity. Many lectins have binding affinity for different types of glycans. For example in this study, WGA and LEL were highly attached to all cell types in 2D, and even to the cell-free scaffolds in the 3D model. This is due to the fact that these two lectins are not only specific for the sugars targeted above, but they additionally have binding pockets specific to other sugar types. In addition to NeuAc (sialic acid on glycosphingolipids and glycoproteins), WGA binds to GlcNAc (N-acetylglucosamine) (Lis and Sharon 1991). Similarly, LEL binds to GlcNAc as well as high mannose *N*-glycans. (Oguri 2005). Human glioblastoma cells (U87-MG) possess high content of GlcNAc on their cell membranes, which is the reason why 2D results indicated that U87-MG cell-lines had attracted the highest amount of WGA. Also, brain ECM contains hyaluronic acid which is composed of alternating GlcNAc monomers, and explains the binding of both WGA and LEL to the scaffolds. However, the binding site of AAL is only specific to fucose containing oligosaccharides but with the highest affinity for core fucose (Yamashita, Kochibe et al. 1985) which explains why AAL did not bind to the surface of the scaffolds that do not contain fucose, and was bound to U87-MG cells which are highly fucosylated and express more fucose on their surface than PC12 and BV2 cells.

All in all, lectins are not as specific as antibody probes that often have high affinity for their targeted moieties, but they are still worth studying. For instance, this study showed that WGA and LEL may bind to acellular scaffolds and all three types of CNS cells in this study randomly. Therefore, they are not appropriate targeting tools for natural 3D brain models. On the other hand, AAL does not bind to the brain ECM and targets fucose exclusively,

especially core fucose, so it can be a potential specific agent for future diagnostic and theranostic studies on brain cancer within natural 3D models or *in vivo*.

4.3 Properties of the 3D Scaffolds

As mentioned in chapter 1, 2D cell culture models have several limitations such as stiffness of the plate and coverslip that affects the shape and function of cells including expression of different proteins, lipids and sugars. In addition, cell adhesion and intercellular signalling is adversely influenced by the flat growth area. All of those changes in cell properties and functions that change, may lead to different results from natural conditions. Therefore, a more ideal environment is required for cells to grow naturally for more realistic experimental results. The 3D scaffolds used in this project are novel model systems that are still under development and discovery. The de-cellularisation methods are being studied and improved by our research group and collaborators. Therefore, detailed information about the properties of the scaffolds is not yet complete. We are working hard as a team to develop a standard 3D model to study brain and other organ cells in a more naturally occurring environment for the cells. One of the facts about the 3D model is that the scaffolds show heterogeneity and looked different in various areas when imaged using scanning electron microscope by other team members. Some believe that this is advantageous because it is more natural and realistic while others argue that it might cause issues with comparing different conditions of an experiment and control samples. However, they were proudly utilised in this study as another step towards understanding the benefits and drawbacks of the scaffolds for cell growth and treatments with nanoparticles. Mass spectrometry analysis by another team member showed that many of the glycoproteins and glycolipids of the ECM have been preserved in these scaffolds. The issue with this kind of analysis is that the results come from a protein or lipid mixture and are not localised. Therefore, it is not possible to speculate whether the glycolipids or the glycoproteins exist in the area of the study or not, which can lead to wrong comparison of results and conclusions. Hence, future precise imaging studies about the location and amount of molecules in different areas of the scaffolds, such as matrix-assisted laser desorption/ionization imaging (Gustafsson, Briggs et al. 2014), are required.

4.4 FND-Lectin Conjugations and the 3D Constructs

Regardless of the location and amount of those glycoconjugates, the results of this study showed very low or even no binding of FND-lectins to the 3D constructs, as compared to 2D results. The difference between FND-lectin and FITC-lectin in 3D could be due to the green autofluorescence of the scaffolds which could have been combined with the green FITC

fluorescence during the intensity measurements. If that is the case, it is difficult to say whether FITC-lectin was attached to the cells. Hence, it can be concluded that the results of 2D and 3D experiments are completely different, so any findings from 2D lectin binding to cells could be entirely different if tested in 3D cell growth. For avoiding such problems in the future, using a different fluorophore with a distinct emission to the auto-fluorescence of the scaffolds and cells, or using time-gated microscopy which is a method to eliminate auto-fluorescence are recommended.

The dissimilarity of the 2D and 3D results may also be based on other reasons such as the settlement of the bio-conjugated nanodiamonds at the bottom due to their weight. In a 2D flask, cells are distributed at the bottom of the flask in a single layer, while in the 3D model the cells are multilayered and on top of each other in the scaffold. When the lectin-conjugated nanodiamonds are added with a pipette from above, their weight settles them at the bottom. Therefore, in the 2D model most of the single-layer cells steadily take them in, while in the 3D model the top layers have a lower opportunity to interact with the bio-conjugated nanodiamonds before their settlement at the bottom because of their weight. Another reason could be the size of the nanodiamonds bio-conjugated with lectins could have been too large to penetrate the scaffolds and reach to the cells (Belli, Guarnieri et al. 2017). However, the DLS measurement showed that after sonication the bio-conjugated nanodiamonds were almost 150 nm, and particles with sizes between 100-200 nm have been shown to pass through the tight junctions of the blood brain barrier (Ben-Zvi, Lacoste et al. 2014). A third reason may be the selectivity of lectins that targets specific binding to the scaffolds or the surface of the cells by the nanodiamonds, and therefore reduces entrance into the cells. This hypothesis is backed by the experiments that showed the entrance of raw nanodiamonds (without any lectins) is greater than bio-conjugated nanodiamonds in both 2D and 3D grown cells (Figures 20, 25 and Appendix figure). The final possible reason for reduced FND-lectin binding may be that the nanodiamonds were trapped in the structures of the 3D scaffolds with their macromolecules especially collagen, restricting them from moving freely as they do in 2D culture; this has been previously observed with other types of nanoparticles (Netti, Berk et al. 2000).

4.5 Staining Method for 3D Microscopy

The treatment and staining of the 2D cells were simple and straight forward. The cells were first treated with either lectin-FITC (green labels) or lectin-FND (red labels) for 24 hours, and then their nuclei were stained with NucBlue mounting oil on the slides. However, the staining of the 3D samples was complicated and confused by using phalloidin to try to

differentiate the cells from the scaffolds. Nanodiamonds emit red light and FITC emits green light; therefore, it was important to use opposite emission colours with Phalloidin depending on the treatment. For that reason, Phalloidin-Alexafluor594 (red emission) was used with FITC labelled samples and Phalloidin-Alexafluor488 (green emission) was used with FND labelled samples. In some samples the green colour of FITC and the red colour of Phalloidin-Alexafluor594 interfered due to co-localisation of f-actin filaments and stained sugars. This is an instance where a lectin can be used for detection and investigation of the presence of a sugar on the surface of a cell. This is just based on a simple observation and needs thorough investigation. However, it shows how challenging the choice of the staining material can be. For this reason, it is recommended to use another product that includes cyan fluorescent protein (CFP) for staining the plasma membrane of the cells. For instance, CellLight® Plasma Membrane-CFP, BacMam 2.0 (catalogue number: C10606) can be utilised, which can be excited by ultraviolet light and will emit in DAPI channel in blue, with a chance of overlap in green with FITC. The benefits of using this product for a similar study would be that the different labelled cells can be differentiated. In addition, Phalloidin targets the entire cytoskeleton plus the f-actins that connect the cells to the matrix, while CFP stains only the plasma membrane of the cells. The drawbacks of this product compared to Phalloidin-Alexafluor would be that it needs overnight or in case of neurons up to 5 days of incubation in order for it to transfect and stain the cell membrane, while the Phalloidin-Alexafluor stains only need 30 minutes of incubation, and can be imaged immediately after the incubation. Moreover, CFP excitation and emission spectra are between that of DAPI and FITC, so DAPI and FITC channels may both pick up the wavelength of the stain.

4.6 Cell Growth Patterns in the Constructs

The microscopic images of 3D constructs show that U87-MG cell lines have grown in a consistent pattern in the scaffolds, while PC12 cells did not grow in some parts of the scaffolds, leaving empty areas among the cells, and BV2 cell lines seemed to have damaged some parts of the scaffolds (figure 26).

U87-MG are malignant glioblastoma cancer cells; therefore, they grow and migrate through the tissues very fast. It is in their nature to adapt to new tissues regardless of their properties and continue growing, which could be a reason for their homogenic distribution all over the scaffold.

PC12 cells represent neurons, and neurons do not grow at the blood brain barrier in live organisms. In fact, astrocytes grow near those areas to protect neurons and maintain the

blood brain barrier. Those empty areas could be therefore the placeholders for blood vessels and epithelial cells, where neurons are not designed to adhere.

BV2 cells are mouse microglial cells; microglia's role in the brain is similar to the role of macrophages, phagocytosis of stranger molecules. The scaffolds were de-cellularised from sheep brain tissue and could be counted as stranger molecules to mouse microglia. Therefore, the torn-up areas of the scaffolds can be due to phagocytosis by BV2 cells.

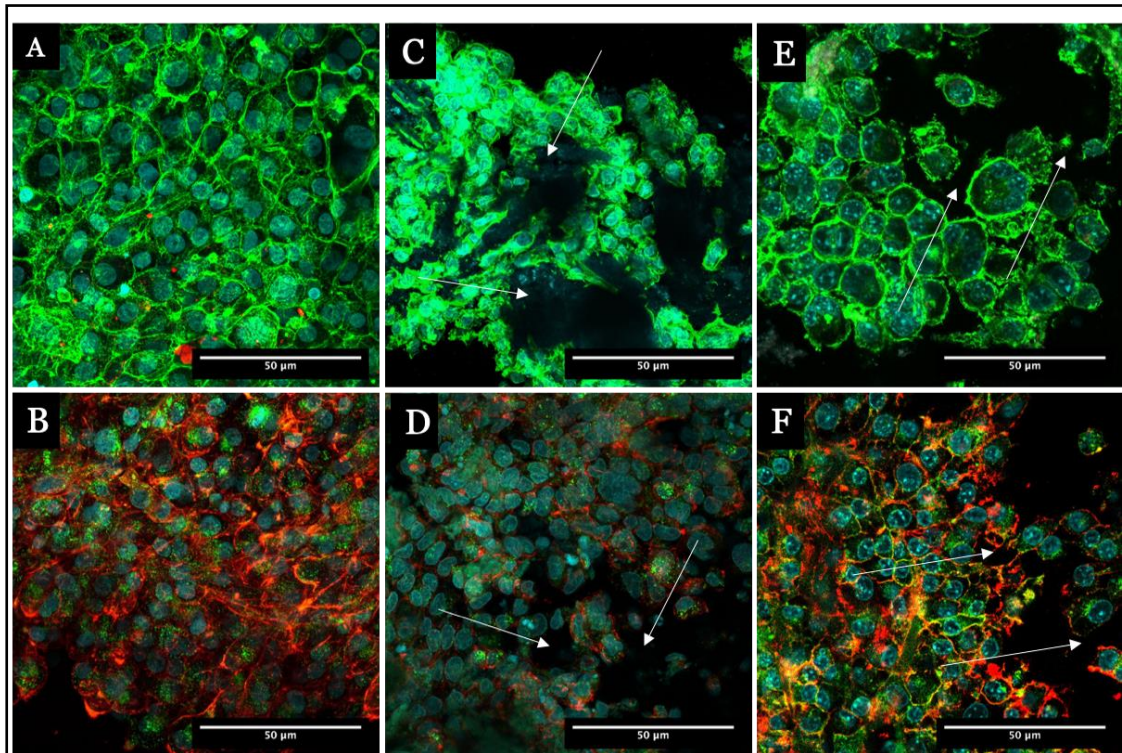


Figure 26. Growth of different CNS cell lines in the acellular 3D scaffolds. The images above show the growth pattern of astrocytes, neurons and microglia in the decellularized scaffolds. **A** and **B**. Astrocytes have grown in a consistent pattern. **C** and **D**. Neurons did not grow in some parts of the scaffolds leaving them empty (shown by white arrows). **E** and **F**. microglia cells seem to have damaged some areas of the scaffolds in addition to not growing in those areas (shown with white arrows).

4.7 Developing 3D Brain Models for Sugar Receptor Targeting with Bio-conjugated Nanodiamonds and the Future Perspectives

The project for developing 3D brain models for cell surface sugar targeting with bio-conjugated nanodiamonds was not as straight forward as expected. Problems with bio-conjugation of nanodiamonds with lectins, the multiple binding sites of lectins for different sugars, cell growth issues in the scaffolds and struggling with characterisation of scaffold properties, in addition to finding a suitable staining method for 3D cell cultures have all caused challenges throughout the pathway. Despite all these problems and challenges, some

worthy results have been risen from these experiments. The scaffolds are very good platforms for the growth of U87-MG glioblastoma astrocytes, and they have attached AAL lectin much more than the other two cell-lines of the study. Although FNDs were not taken up by the 3D constructs in general, U87-MG constructs attracted more nanodiamonds than the other cell lines grown in 3D in general. Optimisation of this method may be helpful for the future of glioblastoma multiforme cancer treatment studies. Drugs can be loaded onto the AAL conjugated nanodiamonds and delivered to U87-MG cells in 3D cell growth to study the absorption, remaining time in the cells, and effects of the drugs on the tumours.

Chapter 5: Summary and Conclusion

The overall aim of this project was to develop a 3D cellular growth model for targeting sugars on the surface of different CNS cells by using lectins (carbohydrate recognising proteins) that are conjugated to nanodiamonds. The several stages of this study included bio-conjugation of nanodiamonds with lectins, culturing cells in 2D, making 3D scaffolds from natural brain tissues, culturing cells in these 3D scaffolds, treatment of the cultured cells in 2D and 3D with labelled-lectins (targeting cell surface sugars), confocal microscopy, and data analysis. Firstly, the high-pressure high-temperature raw nanodiamonds were bio-conjugated with three different lectins (AAL, WGA and LEL) and then characterised for the attachment and aggregation state. Then, three different brain cell-lines (U87-MG, PC12 and BV2) were cultured in 2D flasks for comparison with their growth in the 3D model. To prepare a 3D scaffold for cell growth, sheep brain tissues were prepared by a decellularisation process and were cut into smaller pieces and sterilised. Then, 100,000 cells were seeded on each scaffold and grown for two weeks. The cultured cells from 2D and 3D growth were then treated with nanodiamond-labelled lectins, and also with FITC-labelled lectins, as the classic labelling model, for comparison of the results from the nanodiamond study. After 24-48 hours, cells were fixed, then either mounted on a slide with NucBlue mounting oil or stained with Phalloidin and NucBlue in their well plates, depending on being 2D or 3D cultured cells. Then, the samples were imaged using a confocal microscope, the fluorescent intensity of labelled cells in the images was analysed using Imaris software and finally comparison graphs were made from the data using GraphPad software.

The popularity of different 3D cell culture methods is increasing because they reflect a different and more realistic imitation of natural cell growth and intracellular pathways, compared to 2D cell culture models. The 3D models are also preferred to *in-vivo* experiments, firstly due to moral and ethical issues with animal testing, and secondly owing to the option of studying a single cell type behaviour at a time. The latter reason enables the researchers to examine and compare the results of stimulating different cell types of a specific tissue with the same agent, which is similar to the benefits of *in-vitro* 2D cell cultures. It becomes critical to know how each individual cell type reacts to a stimulation when the research is about targeting cell lines for theranostic purposes or personal medicine studies, where biomarkers can be discovered and targeted for imaging, diagnostics and drug delivery. There are several 3D cell culture methods developed up to date as mentioned in the

first chapter. Among them, natural acellular tissue engineering is selected for this study because it is closer to *in-vivo* conditions.

Abnormal glycosylation of brain cells is reported in many of the diseases associated with brain cells. Those data can be used to find unique targets on the diseased cells in the brain, so that suitable drugs can be delivered to the selectively targeted cells. Lectins have specific binding sites for sugars, which makes them suitable for selective targeting of cells with the abnormal cell surface glycosylation. AAL, WGA and LEL were selected for targeting fucose, sialic acid and high mannose structures on the surfaces of U87-MG, PC12 and BV2 cell lines. However, some lectins have specificity for more than only one type of sugar residue. For example in this study, WGA and LEL both show specificity for GlcNAc in addition to the mentioned sugars, whilst AAL has specificity for only one type of sugar, fucose. Therefore, WGA and LEL were found to target both the 3D scaffolds structures and the cells growing in the scaffolds, because GlcNAc is present in the structure of hyaluronic acid of brain extracellular matrix. Importantly, AAL did not target the scaffolds as fucose is not a component of brain extracellular matrix.

To investigate and image the binding of these lectins to the 2D cells and 3D cell growth constructs, lectins were labelled with 2 different probes, nanodiamonds and FITC dye that emit red and green fluorescence correspondingly. Both the 2D grown cells and the 3D scaffolds before cell inoculation were found to have high background fluorescent intensity in this study, that made it difficult to differentiate the green cellular autofluorescence from the FITC fluorescence, while nanodiamonds did stand out as bright and shiny little particles distinct from the overall red cellular autofluorescence. Therefore, FITC is not recommended as an imaging and diagnostic label with brain cells, because it can be mistaken with the autofluorescence of the cells, while nanodiamonds can be better distinguished.

Overall, there were many lessons learnt through this research project, and there is still much room for optimisation and standardisation of the methods. To summarise, lectins bound to FNDs do not attach as well to 3D grown cells in brain scaffolds compared to high attachment to 2D cells, in general. All FITC and FND conjugated lectins bound well to all the brain cell types with different intensities when grown in 2D culture. In the 3D cell growth scaffold model, FITC conjugated lectins suffered from interference from autofluorescence so quantitation was compromised. Interestingly however, in 3D grown cells only the AAL lectin was not interfered with by the scaffold binding and this lectin bound only to the U87-MG cells and not to the PC12 or BV2 cells, thus providing an important differentiation of astrocytes from other brain cell types for future targeting.

References

- Adamczyk, B., T. Tharmalingam and P. M. Rudd (2012). "Glycans as cancer biomarkers." *Biochim Biophys Acta* **1820**(9): 1347-1353.
- Ahmad, Z., A. Shah, M. Siddiq and H.-B. Kraatz (2014). "Polymeric micelles as drug delivery vehicles." *RSC Adv.* **4**(33): 17028-17038.
- Ajit Varki, E. E., Richard D Cummings, and P. S. Jeffrey D Esko, Gerald W Hart, Markus Aebi, Alan G Darvill, Taroh Kinoshita, Nicolle H Packer, James H Prestegard, Ronald L Schnaar, Peter H Seeberger (2015-2017). *Essentials of Glycobiology* (Internet). E. E. Ajit Varki, Richard D Cummings, Jeffrey D Esko, Pamela Stanley, Gerald W Hart, Markus Aebi, Alan G Darvill, Taroh Kinoshita, Nicolle H Packer, James H Prestegard, Ronald L Schnaar, Peter H Seeberger. Cold Spring Harbor (NY), Cold Spring Harbor Laboratory Press.
- Amoureux, M. C., B. Coulibaly, O. Chinot, A. Loundou, P. Metellus, G. Rougon and D. Figarella-Branger (2010). "Polysialic acid neural cell adhesion molecule (PSA-NCAM) is an adverse prognosis factor in glioblastoma, and regulates olig2 expression in glioma cell lines." *BMC Cancer* **10**: 91.
- Anna Guller, I. T., Elena Petersen, Anatoly Shekhter, Alexander Kurkov, and A. Z. Yi Qian (2015). "Acellular organ scaffolds for tumor tissue engineering." *Micro+Nano Materials, Devices, and Systems* **9668**.
- Badylak, S. F. (2004). "Xenogeneic extracellular matrix as a scaffold for tissue reconstruction." *Transpl Immunol* **12**(3-4): 367-377.
- Bae, Y. H. and K. Park (2011). "Targeted drug delivery to tumors: Myths, reality and possibility." *Journal of Controlled Release* **153**(3): 198-205.
- Barenholz, Y. (2012). "Doxil(R)--the first FDA-approved nano-drug: lessons learned." *J Control Release* **160**(2): 117-134.
- Barras, A., S. Szunerits, L. Marcon, N. Monfilliette-Dupont and R. Boukherroub (2010). "Functionalization of diamond nanoparticles using "click" chemistry." *Langmuir* **26**(16): 13168-13172.
- Belli, V., D. Guarnieri, M. Biondi, F. Della Sala and P. A. Netti (2017). "Dynamics of nanoparticle diffusion and uptake in three-dimensional cell cultures." *Colloids Surf B Biointerfaces* **149**: 7-15.
- Ben-Zvi, A., B. Lacoste, E. Kur, B. J. Andreone, Y. Mayshar, H. Yan and C. Gu (2014). "Mfsd2a is critical for the formation and function of the blood-brain barrier." *Nature* **509**(7501): 507-511.
- Bertrand, N., J. Wu, X. Xu, N. Kamaly and O. C. Farokhzad (2014). "Cancer nanotechnology: The impact of passive and active targeting in the era of modern cancer biology." *Advanced Drug Delivery Reviews* **66**: 2-25.
- Bielecka, Z. F., K. Maliszewska-Olejniczak, I. J. Safir, C. Szczylik and A. M. Czarnecka (2017). "Three-dimensional cell culture model utilization in cancer stem cell research." *Biol Rev Camb Philos Soc* **92**(3): 1505-1520.
- Bott, K., Z. Upton, K. Schrobback, M. Ehrbar, J. A. Hubbell, M. P. Lutolf and S. C. Rizzi (2010). "The effect of matrix characteristics on fibroblast proliferation in 3D gels." *Biomaterials* **31**(32): 8454-8464.
- Bradac, C., J. M. Say, I. D. Rastogi, N. M. Cordina, T. Volz and L. J. Brown (2016). "Nano-assembly of nanodiamonds by conjugation to actin filaments." *J Biophotonics* **9**(3): 296-304.
- Brandley, B. K. and R. L. Schnaar (1986). "Cell-surface carbohydrates in cell recognition and response." *J Leukoc Biol* **40**(1): 97-111.
- Burns, J. S., W.-D. Lü, L. Zhang, C.-L. Wu, Z.-G. Liu, G.-Y. Lei, J. Liu, W. Gao and Y.-R. Hu (2014). "Development of an Acellular Tumor Extracellular Matrix as a Three-Dimensional Scaffold for Tumor Engineering." *PLoS ONE* **9**(7).

18. Chaubey, A., K. J. Ross, R. M. Leadbetter and K. J. Burg (2008). "Surface patterning: tool to modulate stem cell differentiation in an adipose system." J Biomed Mater Res B Appl Biomater **84**(1): 70-78.
19. Chen, X. and W. Zhang (2017). "Diamond nanostructures for drug delivery, bioimaging, and biosensing." Chem Soc Rev **46**(3): 734-760.
20. Chik, J. H., J. Zhou, E. S. Moh, R. Christopherson, S. J. Clarke, M. P. Molloy and N. H. Packer (2014). "Comprehensive glycomics comparison between colon cancer cell cultures and tumours: implications for biomarker studies." J Proteomics **108**: 146-162.
21. Chitcholtan, K., E. Asselin, S. Parent, P. H. Sykes and J. J. Evans (2013). "Differences in growth properties of endometrial cancer in three dimensional (3D) culture and 2D cell monolayer." Exp Cell Res **319**(1): 75-87.
22. Chow, E. K., X. Q. Zhang, M. Chen, R. Lam, E. Robinson, H. Huang, D. Schaffer, E. Osawa, A. Goga and D. Ho (2011). "Nanodiamond therapeutic delivery agents mediate enhanced chemoresistant tumor treatment." Sci Transl Med **3**(73): 73ra21.
23. Collins, A. T. (2002). "The Fermi level in diamond." Journal of Physics: Condensed Matter **14**(14): 3743-3750.
24. Collins, B. E. and J. C. Paulson (2004). "Cell surface biology mediated by low affinity multivalent protein-glycan interactions." Curr Opin Chem Biol **8**(6): 617-625.
25. Coluccia, D., C. A. Figueiredo, M. Y. Wu, A. N. Riemenschneider, R. Diaz, A. Luck, C. Smith, S. Das, C. Ackerley, M. O'Reilly, K. Hynynen and J. T. Rutka (2018). "Enhancing glioblastoma treatment using cisplatin-gold-nanoparticle conjugates and targeted delivery with magnetic resonance-guided focused ultrasound." Nanomedicine **14**(4): 1137-1148.
26. Cordina, N. M., N. Sayyadi, L. M. Parker, A. Everest-Dass, L. J. Brown and N. H. Packer (2018). "Reduced background autofluorescence for cell imaging using nanodiamonds and lanthanide chelates." Sci Rep **8**(1): 4521.
27. Coune, A. (1988). "Liposomes as drug delivery system in the treatment of infectious diseases potential applications and clinical experience." Infection **16**(3): 141-147.
28. Cukierman, E., R. Pankov, D. R. Stevens and K. M. Yamada (2001). "Taking cell-matrix adhesions to the third dimension." Science **294**(5547): 1708-1712.
29. Datta, N. R., S. Krishnan, D. E. Speiser, E. Neufeld, N. Kuster, S. Bodis and H. Hofmann (2016). "Magnetic nanoparticle-induced hyperthermia with appropriate payloads: Paul Ehrlich's "magic (nano)bullet" for cancer theranostics?" Cancer Treat Rev **50**: 217-227.
30. De Mejia, E. G. and V. I. Prisecaru (2005). "Lectins as bioactive plant proteins: a potential in cancer treatment." Crit Rev Food Sci Nutr **45**(6): 425-445.
31. Diamandis, E. P. (2012). "The failure of protein cancer biomarkers to reach the clinic: why, and what can be done to address the problem?" BMC Med **10**: 87.
32. Dolmatov, V. Y. (2001). "Detonation synthesis ultradispersed diamonds: properties and applications." Russian Chemical Reviews **70**(7): 607-626.
33. Duval, K., H. Grover, L. H. Han, Y. Mou, A. F. Pegoraro, J. Fredberg and Z. Chen (2017). "Modeling Physiological Events in 2D vs. 3D Cell Culture." Physiology (Bethesda) **32**(4): 266-277.
34. Eggleton, B. J., S. Palomba, A. Guller, I. Trusova, E. Petersen, A. Shekhter, A. Kurkov, Y. Qian and A. Zvyagin (2015). Acellular organ scaffolds for tumor tissue engineering. Micro+Nano Materials, Devices, and Systems.
35. Fang, Y. and R. M. Eglén (2017). "Three-Dimensional Cell Cultures in Drug Discovery and Development." SLAS Discov **22**(5): 456-472.
36. Fennema, E., N. Rivron, J. Rouwkema, C. van Blitterswijk and J. de Boer (2013). "Spheroid culture as a tool for creating 3D complex tissues." Trends Biotechnol **31**(2): 108-115.
37. Freysd'ottir, J. (2000). "Production of monoclonal antibodies." Methods Mol Med **40**: 267-279.

38. Gabius, H. J., S. Andre, J. Jimenez-Barbero, A. Romero and D. Solis (2011). "From lectin structure to functional glycomics: principles of the sugar code." Trends Biochem Sci **36**(6): 298-313.
39. Gjorevski, N., A. S. Piotrowski, V. D. Varner and C. M. Nelson (2015). "Dynamic tensile forces drive collective cell migration through three-dimensional extracellular matrices." Sci Rep **5**: 11458.
40. Grinnell, F. (2003). "Fibroblast biology in three-dimensional collagen matrices." Trends in Cell Biology **13**(5): 264-269.
41. Guruswamy Damodaran, R. and P. Vermette (2018). "Decellularized pancreas as a native extracellular matrix scaffold for pancreatic islet seeding and culture." J Tissue Eng Regen Med.
42. Gustafsson, O. J. R., M. T. Briggs, M. R. Condina, L. J. Winderbaum, M. Pelzing, S. R. McColl, A. V. Everest-Dass, N. H. Packer and P. Hoffmann (2014). "MALDI imaging mass spectrometry of N-linked glycans on formalin-fixed paraffin-embedded murine kidney." Analytical and Bioanalytical Chemistry **407**(8): 2127-2139.
43. Haley, B. and E. Frenkel (2008). "Nanoparticles for drug delivery in cancer treatment." Urol Oncol **26**(1): 57-64.
44. Hewitt, S. M. (2004). "Discovery of Protein Biomarkers for Renal Diseases." Journal of the American Society of Nephrology **15**(7): 1677-1689.
45. Holt, K. B. (2007). "Diamond at the nanoscale: applications of diamond nanoparticles from cellular biomarkers to quantum computing." Philosophical Transactions of the Royal Society A: Mathematical, Physical and Engineering Sciences **365**(1861): 2845-2861.
46. Huang, H., E. Pierstorff, E. Osawa and D. Ho (2007). "Active nanodiamond hydrogels for chemotherapeutic delivery." Nano Lett **7**(11): 3305-3314.
47. Hughes, G. A. (2005). "Nanostructure-mediated drug delivery." Dis Mon **51**(6): 342-361.
48. Iakoubovskii, K. and A. T. Collins (2004). "Alignment of Ni- and Co-related centres during the growth of high-pressure-high-temperature diamond." Journal of Physics: Condensed Matter **16**(39): 6897-6906.
49. Iwasaki, T., F. Ishibashi, Y. Miyamoto, Y. Doi, S. Kobayashi, T. Miyazaki, K. Tahara, K. D. Jahnke, L. J. Rogers, B. Naydenov, F. Jelezko, S. Yamasaki, S. Nagamachi, T. Inubushi, N. Mizuochi and M. Hatano (2015). "Germanium-Vacancy Single Color Centers in Diamond." Sci Rep **5**: 12882.
50. Iyer, A. K., G. Khaled, J. Fang and H. Maeda (2006). "Exploiting the enhanced permeability and retention effect for tumor targeting." Drug Discovery Today **11**(17-18): 812-818.
51. Jain, K. K. (2007). "Nanobiotechnology-based drug delivery to the central nervous system." Neurodegener Dis **4**(4): 287-291.
52. Jäkel, S. and L. Dimou (2017). "Glial Cells and Their Function in the Adult Brain: A Journey through the History of Their Ablation." Frontiers in Cellular Neuroscience **11**.
53. Kaur, R. and I. Badea (2013). "Nanodiamonds as novel nanomaterials for biomedical applications: drug delivery and imaging systems." Int J Nanomedicine **8**: 203-220.
54. Khalid, A., A. N. Mitropoulos, B. Marelli, S. Tomljenovic-Hanic and F. G. Omenetto (2016). "Doxorubicin loaded nanodiamond-silk spheres for fluorescence tracking and controlled drug release." Biomed Opt Express **7**(1): 132-147.
55. Köhler, G. and C. Milstein (1975). "Continuous cultures of fused cells secreting antibody of predefined specificity." Nature **256**(5517): 495-497.
56. Kreuter, J. (2007). "Nanoparticles--a historical perspective." Int J Pharm **331**(1): 1-10.
57. Krukemeyer, M., V. Krenn and F. Huebner (2015). "History and Possible Uses of Nanomedicine Based on Nanoparticles and Nanotechnological Progress." Journal of Nanomedicine & Nanotechnology **06**(06).

58. Kumar, S., M. Saxena, K. Srinivas and V. K. Singh (2015). "Fucose: A biomarker in grading of oral cancer." Natl J Maxillofac Surg **6**(2): 176-179.
59. Lamichhane, N., T. S. Udayakumar, W. D. D'Souza, C. B. Simone, 2nd, S. R. Raghavan, J. Polf and J. Mahmood (2018). "Liposomes: Clinical Applications and Potential for Image-Guided Drug Delivery." Molecules **23**(2).
60. Lefranc, F., J. Brotchi and R. Kiss (2005). "Possible Future Issues in the Treatment of Glioblastomas: Special Emphasis on Cell Migration and the Resistance of Migrating Glioblastoma Cells to Apoptosis." Journal of Clinical Oncology **23**(10): 2411-2422.
61. Lenman, A., A. M. Liaci, Y. Liu, L. Frangmyr, M. Frank, B. S. Blaum, W. Chai, Podgorski, II, B. Harrach, M. Benko, T. Feizi, T. Stehle and N. Arnberg (2018). "Polysialic acid is a cellular receptor for human adenovirus 52." Proc Natl Acad Sci U S A **115**(18): E4264-E4273.
62. Li, J., Y. Zhu, W. Li, X. Zhang, Y. Peng and Q. Huang (2010). "Nanodiamonds as intracellular transporters of chemotherapeutic drug." Biomaterials **31**(32): 8410-8418.
63. Liao, H., J. Wu, E. Kuhn, W. Chin, B. Chang, M. D. Jones, S. O'Neil, K. R. Clauser, J. Karl, F. Hasler, R. Roubenoff, W. Zolg and B. C. Guild (2004). "Use of mass spectrometry to identify protein biomarkers of disease severity in the synovial fluid and serum of patients with rheumatoid arthritis." Arthritis Rheum **50**(12): 3792-3803.
64. Lin, C. L., C. H. Lin, H. C. Chang and M. C. Su (2015). "Protein Attachment on Nanodiamonds." J Phys Chem A **119**(28): 7704-7711.
65. Lis, H. and N. Sharon (1991). "Lectin-carbohydrate interactions." Current Opinion in Structural Biology **1**(5): 741-749.
66. Liu, W., M. Howarth, A. B. Greytak, Y. Zheng, D. G. Nocera, A. Y. Ting and M. G. Bawendi (2008). "Compact biocompatible quantum dots functionalized for cellular imaging." J Am Chem Soc **130**(4): 1274-1284.
67. Liu, X., V. Gurel, D. Morris, D. W. Murray, A. Zhitkovich, A. B. Kane and R. H. Hurt (2007). "Bioavailability of Nickel in Single-Wall Carbon Nanotubes." Advanced Materials **19**(19): 2790-2796.
68. Liu, X., H. Nie, Y. Zhang, Y. Yao, A. Maitikabili, Y. Qu, S. Shi, C. Chen and Y. Li (2013). "Cell surface-specific N-glycan profiling in breast cancer." PLoS One **8**(8): e72704.
69. Liu, Y., Y. Zhao, B. Sun and C. Chen (2013). "Understanding the Toxicity of Carbon Nanotubes." Accounts of Chemical Research **46**(3): 702-713.
70. Mabry, K. M., S. Z. Payne and K. S. Anseth (2016). "Microarray analyses to quantify advantages of 2D and 3D hydrogel culture systems in maintaining the native valvular interstitial cell phenotype." Biomaterials **74**: 31-41.
71. Man, H. B., H. Kim, H. J. Kim, E. Robinson, W. K. Liu, E. K. Chow and D. Ho (2014). "Synthesis of nanodiamond-daunorubicin conjugates to overcome multidrug chemoresistance in leukemia." Nanomedicine **10**(2): 359-369.
72. Merkel, T. J. and J. M. DeSimone (2011). "Dodging Drug-Resistant Cancer with Diamonds." Science Translational Medicine **3**(73): 73ps78-73ps78.
73. Merson, T. D., S. Castelletto, I. Aharonovich, A. Turbic, T. J. Kilpatrick and A. M. Turnley (2013). "Nanodiamonds with silicon vacancy defects for nontoxic photostable fluorescent labeling of neural precursor cells." Opt Lett **38**(20): 4170-4173.
74. Millipore, E. (2012). "Precise and Accurate Counts and Viability Measurements Across Multiple Cell Lines Using the Muse™ Cell Count & Viability Assay." BioTechniques **52**(3): 200-203.
75. Miyoshi, E., K. Moriwaki, N. Terao, C. C. Tan, M. Terao, T. Nakagawa, H. Matsumoto, S. Shinzaki and Y. Kamada (2012). "Fucosylation is a promising target for cancer diagnosis and therapy." Biomolecules **2**(1): 34-45.
76. Mochalin, V. N., O. Shenderova, D. Ho and Y. Gogotsi (2011). "The properties and applications of nanodiamonds." Nat Nanotechnol **7**(1): 11-23.
77. Mudshinge, S. R., A. B. Deore, S. Patil and C. M. Bhalgat (2011). "Nanoparticles: Emerging carriers for drug delivery." Saudi Pharm J **19**(3): 129-141.

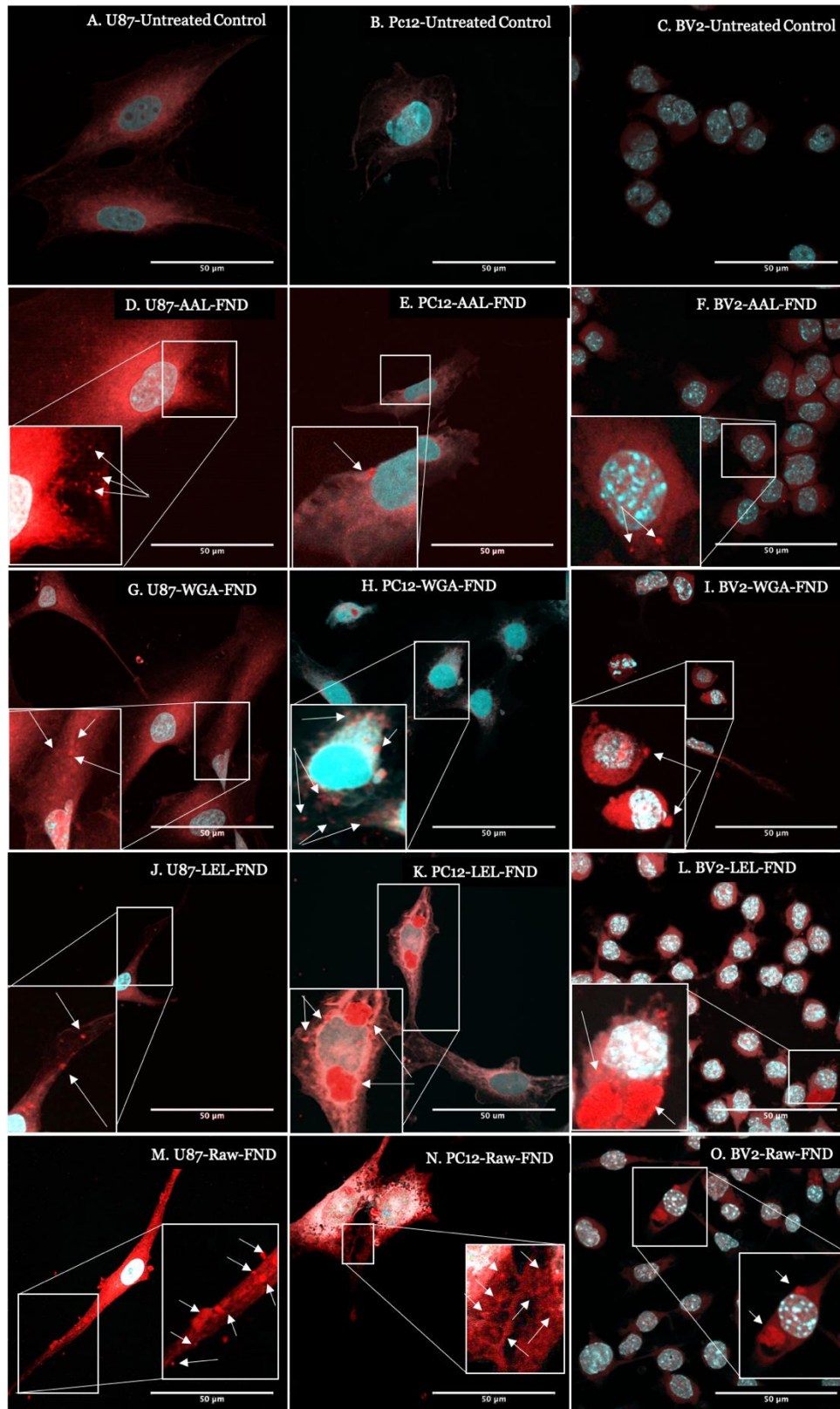
78. Nag, O. K. and V. Awasthi (2013). "Surface engineering of liposomes for stealth behavior." Pharmaceutics **5**(4): 542-569.
79. Netti, P. A., D. A. Berk, M. A. Swartz, A. J. Grodzinsky and R. K. Jain (2000). "Role of Extracellular Matrix Assembly in Interstitial Transport in Solid Tumors." Cancer Res **60**(9): 2497-2503.
80. Norton, P., M. A. Comunale, H. Herrera, M. Wang, J. Houser, M. Wimmerova, P. R. Romano and A. Mehta (2016). "Development and application of a novel recombinant Aleuria aurantia lectin with enhanced core fucose binding for identification of glycoprotein biomarkers of hepatocellular carcinoma." Proteomics **16**(24): 3126-3136.
81. Oguri, S. (2005). "Analysis of sugar chain-binding specificity of tomato lectin using lectin blot: recognition of high mannose-type N-glycans produced by plants and yeast." Glycoconjugate Journal **22**(7-9): 453-461.
82. Oguri, S. (2005). "Analysis of sugar chain-binding specificity of tomato lectin using lectin blot: recognition of high mannose-type N-glycans produced by plants and yeast." Glycoconj J **22**(7-9): 453-461.
83. Olausson, J., L. Tibell, B. H. Jonsson and P. Pahlsson (2008). "Detection of a high affinity binding site in recombinant Aleuria aurantia lectin." Glycoconj J **25**(8): 753-762.
84. Oshinbolu, S., R. Shah, G. Finka, M. Molloy, M. Uden and D. G. Bracewell (2018). "Evaluation of fluorescent dyes to measure protein aggregation within mammalian cell culture supernatants." Journal of Chemical Technology & Biotechnology **93**(3): 909-917.
85. Pal'yanov, N., A. G. Sokol, M. Borzdov and A. F. Khokhryakov (2002). "Fluid-bearing alkaline carbonate melts as the medium for the formation of diamonds in the Earth's mantle: an experimental study." Lithos **60**(3-4): 145-159.
86. Palmerston Mendes, L., J. Pan and V. P. Torchilin (2017). "Dendrimers as Nanocarriers for Nucleic Acid and Drug Delivery in Cancer Therapy." Molecules **22**(9).
87. Pineda, E. T., R. M. Nerem and T. Ahsan (2013). "Differentiation patterns of embryonic stem cells in two- versus three-dimensional culture." Cells Tissues Organs **197**(5): 399-410.
88. Prabhakar, U., H. Maeda, R. K. Jain, E. M. Sevik-Muraca, W. Zamboni, O. C. Farokhzad, S. T. Barry, A. Gabizon, P. Grodzinski and D. C. Blakey (2013). "Challenges and Key Considerations of the Enhanced Permeability and Retention Effect for Nanomedicine Drug Delivery in Oncology." Cancer Research **73**(8): 2412-2417.
89. Qi, L. and X. Gao (2008). "Emerging application of quantum dots for drug delivery and therapy." Expert Opin Drug Deliv **5**(3): 263-267.
90. Reineck, P., D. W. M. Lau, E. R. Wilson, K. Fox, M. R. Field, C. Deeleejojananan, V. N. Mochalin and B. C. Gibson (2017). "Effect of Surface Chemistry on the Fluorescence of Detonation Nanodiamonds." ACS Nano **11**(11): 10924-10934.
91. Remuzzi, A., M. Figliuzzi, B. Bonandrini, S. Silvani, N. Azzollini, R. Nossa, A. Benigni and G. Remuzzi (2017). "Experimental Evaluation of Kidney Regeneration by Organ Scaffold Recellularization." Sci Rep **7**: 43502.
92. Robert Lam, D. H. (2009). "Nanodiamonds as vehicles for systemic and localized drug delivery." Expert Opinion On Drug Delivery **6**(9): 883-895.
93. Roseman, S. (2001). "Reflections on glycobiology." J Biol Chem **276**(45): 41527-41542.
94. Rosenberg, S. A., P. Aebersold, K. Cornetta, A. Kasid, R. A. Morgan, R. Moen, E. M. Karson, M. T. Lotze, J. C. Yang, S. L. Topalian and et al. (1990). "Gene transfer into humans-immunotherapy of patients with advanced melanoma, using tumor-infiltrating lymphocytes modified by retroviral gene transduction." N Engl J Med **323**(9): 570-578.
95. Roy, U., V. Drozd, A. Durygin, J. Rodriguez, P. Barber, V. Atluri, X. Liu, T. G. Voss, S. Saxena and M. Nair (2018). "Characterization of Nanodiamond-based anti-HIV drug Delivery to the Brain." Sci Rep **8**(1): 1603.
96. Ruoslahti, E. (1996). "Brain extracellular matrix." Glycobiology **6**(5): 489-492.

97. Scadden, D. T. (2006). "The stem-cell niche as an entity of action." Nature **441**(7097): 1075-1079.
98. Schnaar, R. L., R. Gerardy-Schahn and H. Hildebrandt (2014). "Sialic acids in the brain: gangliosides and polysialic acid in nervous system development, stability, disease, and regeneration." Physiol Rev **94**(2): 461-518.
99. Schwartz, R. S. (2004). "Paul Ehrlich's magic bullets." N Engl J Med **350**(11): 1079-1080.
100. Sercombe, L., T. Veerati, F. Moheimani, S. Y. Wu, A. K. Sood and S. Hua (2015). "Advances and Challenges of Liposome Assisted Drug Delivery." Front Pharmacol **6**: 286.
101. Sharon, N. (2007). "Lectins: carbohydrate-specific reagents and biological recognition molecules." J Biol Chem **282**(5): 2753-2764.
102. Shenderova, O. A. and G. E. McGuire (2015). "Science and engineering of nanodiamond particle surfaces for biological applications (Review)." Biointerphases **10**(3): 030802.
103. Shetty, R. K., S. K. Bhandary and A. Kali (2013). "Significance of Serum L-fucose Glycoprotein as Cancer Biomarker in Head and Neck Malignancies without Distant Metastasis." J Clin Diagn Res **7**(12): 2818-2820.
104. Shimizu, T., M. Yamato, A. Kikuchi and T. Okano (2003). "Cell sheet engineering for myocardial tissue reconstruction." Biomaterials **24**(13): 2309-2316.
105. Shimoni, O., K. Bray, L. Cheung, I. Aharanovich and S. Valenzuela (2017).
106. Shojaie, S., L. Ermini, C. Ackerley, J. Wang, S. Chin, B. Yeganeh, M. Bilodeau, M. Sambhi, I. Rogers, J. Rossant, C. E. Bear and M. Post (2015). "Acellular lung scaffolds direct differentiation of endoderm to functional airway epithelial cells: requirement of matrix-bound HS proteoglycans." Stem Cell Reports **4**(3): 419-430.
107. Slaughter, B. V., S. S. Khurshid, O. Z. Fisher, A. Khademhosseini and N. A. Peppas (2009). "Hydrogels in regenerative medicine." Adv Mater **21**(32-33): 3307-3329.
108. Solez, K., K. C. Fung, K. A. Saliba, V. L. C. Sheldon, A. Petrosyan, L. Perin, J. F. Burdick, W. H. Fissell, A. J. Demetris and L. D. Cornell (2018). "The bridge between transplantation and regenerative medicine: Beginning a new Banff classification of tissue engineering pathology." Am J Transplant **18**(2): 321-327.
109. Souza, A. G. and I. C. C Ferreira (2016). "Advances in Cell Culture: More than a Century after Cultivating Cells." Journal of Biotechnology & Biomaterials **6**(2).
110. Sperling, R. A. and W. J. Parak (2010). "Surface modification, functionalization and bioconjugation of colloidal inorganic nanoparticles." Philos Trans A Math Phys Eng Sci **368**(1915): 1333-1383.
111. Sreenivasan, V. K. A., W. A. Wan Razali, K. Zhang, R. R. Pillai, A. Saini, D. Denkova, M. Santiago, H. Brown, J. Thompson, M. Connor, E. M. Goldys and A. V. Zvyagin (2017). "Development of Bright and Biocompatible Nanoruby and Its Application to Background-Free Time-Gated Imaging of G-Protein-Coupled Receptors." ACS Appl Mater Interfaces **9**(45): 39197-39208.
112. Srinivas, P. R., B. S. Kramer and S. Srivastava (2001). "Trends in biomarker research for cancer detection." The Lancet Oncology **2**(11): 698-704.
113. Strebhardt, K. and A. Ullrich (2008). "Paul Ehrlich's magic bullet concept: 100 years of progress." Nat Rev Cancer **8**(6): 473-480.
114. Tay, C. Y., M. S. Muthu, S. L. Chia, K. T. Nguyen, S.-S. Feng and D. T. Leong (2016). "Reality Check for Nanomaterial-Mediated Therapy with 3D Biomimetic Culture Systems." Advanced Functional Materials **26**(23): 4046-4065.
115. Theodosis, D. T., R. Bonhomme, S. Vitiello, G. Rougon and D. A. Poulain (1999). "Cell Surface Expression of Polysialic Acid on NCAM Is a Prerequisite for Activity-Dependent Morphological Neuronal and Glial Plasticity." The Journal of Neuroscience **19**(23): 10228-10236.

116. Tong, Y., R. Liu and T. Zhang (2014). "The effect of a detonation nanodiamond coating on the thermal decomposition properties of RDX explosives." Phys Chem Chem Phys **16**(33): 17648-17657.
117. Torchilin, V. P. (2005). "Recent advances with liposomes as pharmaceutical carriers." Nat Rev Drug Discov **4**(2): 145-160.
118. Torisawa, Y. S., A. Takagi, Y. Nashimoto, T. Yasukawa, H. Shiku and T. Matsue (2007). "A multicellular spheroid array to realize spheroid formation, culture, and viability assay on a chip." Biomaterials **28**(3): 559-566.
119. Tsai, Y. C., P. Vijayaraghavan, W. H. Chiang, H. H. Chen, T. I. Liu, M. Y. Shen, A. Omoto, M. Kamimura, K. Soga and H. C. Chiu (2018). "Targeted Delivery of Functionalized Upconversion Nanoparticles for Externally Triggered Photothermal/Photodynamic Therapies of Brain Glioblastoma." Theranostics **8**(5): 1435-1448.
120. Tsuchiya, N., R. Yamanaka, N. Yajima, J. Homma, M. Sano, T. Komata, T. Ikeda, I. Fujimoto, H. Takahashi, R. Tanaka and K. Ikenaka (2005). "Isolation and characterization of an N-linked oligosaccharide that is increased in glioblastoma tissue and cell lines." International Journal of Oncology.
121. Tung, Y. C., A. Y. Hsiao, S. G. Allen, Y. S. Torisawa, M. Ho and S. Takayama (2011). "High-throughput 3D spheroid culture and drug testing using a 384 hanging drop array." Analyst **136**(3): 473-478.
122. Turcheniuk, K. and V. N. Mochalin (2017). "Biomedical applications of nanodiamond (Review)." Nanotechnology **28**(25).
123. Tyrrell, Z. L., Y. Shen and M. Radosz (2010). "Fabrication of micellar nanoparticles for drug delivery through the self-assembly of block copolymers." Progress in Polymer Science **35**(9): 1128-1143.
124. Underhill, G. H. and S. N. Bhatia (2007). "High-throughput analysis of signals regulating stem cell fate and function." Curr Opin Chem Biol **11**(4): 357-366.
125. Urbanska, K., J. Sokolowska, M. Szmids and P. Sysa (2014). "Glioblastoma multiforme - an overview." Contemp Oncol (Pozn) **18**(5): 307-312.
126. Vijayanthimala, V. and H. C. Chang (2009). "Functionalized fluorescent nanodiamonds for biomedical applications." Nanomedicine (Lond) **4**(1): 47-55.
127. van der Laan, K., M. Hasani, T. Zheng and R. Schirhagl (2018). "Nanodiamonds for In Vivo Applications." Small **14**(19): e1703838.
128. VanderMeulen, D. L., V. V. T. S. Prasad and J. R. Moskal (1994). "The identification of glioblastoma-associated, fucose-containing glycoproteins induced by retinoic acid." Molecular and Chemical Neuropathology **21**(2-3): 311-327.
129. Villacampa, N., B. Almolda, B. Gonzalez and B. Castellano (2013). "Tomato lectin histochemistry for microglial visualization." Methods Mol Biol **1041**: 261-279.
130. Vlasov, I. I., A. S. Barnard, V. G. Ralchenko, O. I. Lebedev, M. V. Kanzyuba, A. V. Saveliev, V. I. Konov and E. Goovaerts (2009). "Nanodiamond Photoemitters Based on Strong Narrow-Band Luminescence from Silicon-Vacancy Defects." Advanced Materials **21**(7): 808-812.
131. Walker, J. (1979). "Optical absorption and luminescence in diamond." Reports on Progress in Physics **42**(10): 1605-1659.
132. Walsh, G. and R. Jefferis (2006). "Post-translational modifications in the context of therapeutic proteins." Nat Biotechnol **24**(10): 1241-1252.
133. Wang, S., E. A. Konorev, S. Kotamraju, J. Joseph, S. Kalivendi and B. Kalyanaraman (2004). "Doxorubicin induces apoptosis in normal and tumor cells via distinctly different mechanisms. intermediacy of H₂O₂- and p53-dependent pathways." J Biol Chem **279**(24): 25535-25543.
134. Wohl, S. G., C. W. Schmeer, T. Fries, O. W. Witte and S. Isenmann (2011). "In situ dividing and phagocytosing retinal microglia express nestin, vimentin, and NG2 in vivo." PLoS One **6**(8): e22408.

135. Wrachtrup, J. (2010). "Nanoparticles: Switching blinking on and off." Nat Nanotechnol **5**(5): 314-315.
136. Xing, Y. and L. Dai (2009). "Nanodiamonds for nanomedicine." Nanomedicine (Lond) **4**(2): 207-218.
137. Xue, X. and X.-J. Liang (2012). "Overcoming drug efflux-based multidrug resistance in cancer with nanotechnology." Chinese Journal of Cancer **31**(2): 100-109.
138. Yale, A. R., J. L. Nourse, K. R. Lee, S. N. Ahmed, J. Arulmoli, A. Y. L. Jiang, L. P. McDonnell, G. A. Botten, A. P. Lee, E. S. Monuki, M. Demetriou and L. A. Flanagan (2018). "Cell Surface N-Glycans Influence Electrophysiological Properties and Fate Potential of Neural Stem Cells." Stem Cell Reports **11**(4): 869-882.
139. Yamashita, K., N. Kochibe, T. Ohkura, I. Ueda and A. Kobata (1985). "Fractionation of L-fucose-containing oligosaccharides on immobilized Aleuria aurantia lectin." J Biol Chem **260**(8): 4688-4693.
140. Yoshii, Y., A. Waki, K. Yoshida, A. Kakezuka, M. Kobayashi, H. Namiki, Y. Kuroda, Y. Kiyono, H. Yoshii, T. Furukawa, T. Asai, H. Okazawa, J. G. Gelovani and Y. Fujibayashi (2011). "The use of nanoimprinted scaffolds as 3D culture models to facilitate spontaneous tumor cell migration and well-regulated spheroid formation." Biomaterials **32**(26): 6052-6058.
141. Yu, B., H. C. Tai, W. Xue, L. J. Lee and R. J. Lee (2010). "Receptor-targeted nanocarriers for therapeutic delivery to cancer." Mol Membr Biol **27**(7): 286-298.
142. Yu, S. J., M. W. Kang, H. C. Chang, K. M. Chen and Y. C. Yu (2005). "Bright fluorescent nanodiamonds: no photobleaching and low cytotoxicity." J Am Chem Soc **127**(50): 17604-17605.
143. Yu, Y., A. Alkhawaji, Y. Ding and J. Mei (2016). "Decellularized scaffolds in regenerative medicine." Oncotarget **7**(36): 58671-58683.
144. Zhang, J., X. Xiao, J. Zhu, Z. Gao, X. Lai, X. Zhu and G. Mao (2018). "Lactoferrin- and RGD-comodified, temozolomide and vincristine-coloaded nanostructured lipid carriers for gliomatosis cerebri combination therapy." Int J Nanomedicine **13**: 3039-3051.
145. Zhang, Y., Y. Huang and S. Li (2014). "Polymeric micelles: nanocarriers for cancer-targeted drug delivery." AAPS PharmSciTech **15**(4): 862-871.
146. Zhang, Z., B. Niu, J. Chen, X. He, X. Bao, J. Zhu, H. Yu and Y. Li (2014). "The use of lipid-coated nanodiamond to improve bioavailability and efficacy of sorafenib in resisting metastasis of gastric cancer." Biomaterials **35**(15): 4565-4572.
147. Zhu, J. and R. E. Marchant (2011). "Design properties of hydrogel tissue-engineering scaffolds." Expert Rev Med Devices **8**(5): 607-626.
148. Zhu, T., Q. Tang, Y. Shen, H. Tang, L. Chen and J. Zhu (2015). "An acellular cerebellar biological scaffold: Preparation, characterization, biocompatibility and effects on neural stem cells." Brain Research Bulletin **113**: 48-57.
149. Zhu, Y., J. Li, W. Li, Y. Zhang, X. Yang, N. Chen, Y. Sun, Y. Zhao, C. Fan and Q. Huang (2012). "The biocompatibility of nanodiamonds and their application in drug delivery systems." Theranostics **2**(3): 302-312.

Appendix



2D microscopy with brain cell samples with lectin-FND conjugations and raw nanodiamonds. A, B and C. Not treated with any lectin as negative controls. **D, E and F.** treated with bio-conjugated nanodiamonds. **J, K and L.** treated with raw nanodiamonds. **M, N and O.** treated with raw nanodiamonds. To show the nanodiamonds in a bigger scale, some areas are enlarged by inset zoom in lectin-FND treated cell-line images. The white arrows point at some of detected nanodiamonds. The green channel for these images is blocked to show the nanodiamonds clearly.